

SURFACE LAYER FORMATION ON Pb/Sn ALLOYS

by

Caroline S. Lee

S.B. Materials Science and Engineering
Massachusetts Institute of Technology (May 1993)

Submitted to the Department of Materials
Science and Engineering in partial
fulfillment of the requirements for the Degree of

**MASTER OF SCIENCE
IN MATERIALS SCIENCE AND ENGINEERING**

at the

MASSACHUSETTS INSTITUTE OF TECHNOLOGY

June 1995

©Massachusetts Institute of Technology 1995
All rights reserved.

Signature of Author _____
Department of Materials Science and Engineering
May 12, 1995

Certified By _____
Professor Thomas W. Eagar
POSCO Professor of Materials Science and Engineering
Thesis Supervisor

Accepted By _____
Professor Carl V. Thompson II
Professor of Electronic Materials
Chair, Departmental Committee on Graduate Students

MASSACHUSETTS INSTITUTE
OF TECHNOLOGY

JUL 20 1995

LIBRARIES

SURFACE LAYER FORMATION ON Pb/Sn ALLOYS

by
Caroline S. Lee

Submitted to the Department of Materials Science
and Engineering on May 12, 1995, in partial
fulfillment of the requirement for the degree

MASTER OF SCIENCE IN MATERIALS SCIENCE AND ENGINEERING

ABSTRACT

With recent advances in silicon technology, microprocessor performance is becoming limited by chip-to-package interconnections. Three primary assembly processes, Wirebonding (WB), Tape Automated Bonding (TAB) and Controlled Collapsed Chip Connection (C4), are used. Out of the three assembly processes, this study focuses on C4 technology where a chip is interconnected to a package by a matrix of solder bumps. C4 offers many advantages over WB or TAB, such as a high input/output density and better overall electrical performance.

Pb/Sn bumps are used as connectors in the C4 technology. Pb/Sn solder bumps produced by electroplating were extensively studied. The use of Pb/Sn electroplating process for C4 requires the ability to etch Ball Limiting Metallurgy (BLM) in the presence of Pb/Sn bumps. Therefore, the appropriate etchant needs to be selected. Upon etching, a surface corrosion layer is formed and an appropriate cleaning acid needs to be selected to remove this layer subsequently. This thesis examines surface layer formation on solder bumps, the morphology of the surface layer and surface layer composition.

It was found that the morphology of the surface layer formed on the Pb/Sn Solder bumps is critically dependent on the concentration of the etchant, especially H_2SO_4 . Using a gravimetric test, XPS and AES analysis, PbO containing Sn and S, was identified to be the primary component of the surface layer after the BLM etch. Moreover, the impact of the BLM etch bath on Pb/Sn solder bumps was investigated. The thickness morphology, composition and the growth rate of the layer are critically dependent on S from H_2SO_4 . In H_2O_2 -rich solution, the surface appears to be loosely packed and the growth rate on the surface of the bump was found to be reaction-rate limited; whereas, in H_2SO_4 -rich solution, the diffusion rate is the controlling step in forming the surface layer on the solder bumps. Also, the layer was thin and dense. Moreover, from the AES scan and the concentration variation of the BLM etch studies, the optimal concentration was determined to be 86% H_2SO_4 solution which results in very slow surface layer growth, limited by the diffusion rate. Using that concentration, BLM etch rates in vertical and lateral directions were studied. The overall etch rate in the lateral direction was determined to be 3 $\mu\text{m}/\text{min}$; whereas, the vertical etch rate was about 1.5 $\mu\text{m}/\text{min}$, thus the etch rate is anisotropic.

Further research needs to be focused on the BLM etch rate studies and on developing better methods for measuring thickness and solubility.

Thesis Supervisors: Professor Thomas Eagar, POSCO Professor of Materials Engineering
Mr. Doug Crafts, Senior Engineer, Intel Corp., Santa Clara, CA

Acknowledgements

Over a period of 7 months of research, engineering, writing resulted in this document. Without substantial help and support from others, this thesis would not been possible to complete. I would like to take this opportunity to thank those who have contributed much to the completion of my Master's thesis.

I wish to express my sincere thanks to my MIT adviser, Professor Thomas Eagar. Even though my experimental work was carried out at Intel, CA, he was always available for me to contact, and he provided critical guidance during this work. I appreciate his technical support, understanding and time spent in proofreading my thesis.

I greatly acknowledge the support and the help of my Intel Supervisors, Mr. Doug Crafts and Dr. V. Murali. Their supports ranged from having "one-on-one" discussions to proofreading my thesis. I really appreciate their technical advices, encouragement and support. I would like to recognize Intel Inc. for the use of laboratories and libraries, as well as accepting me as part of the team. I would like to thank Peter Coon for helping me analyzing Spectroscopic data.

Thanks to Advanced Interconnects Technology Development (AITD) Group members at Intel Inc. for their kindness and emotional supports.

I would also like to thank my friends, Yukyong, Jung-Sul, Christine and Woojun for cheering me up and encouraging me in bad times.

Special thanks to my Parents and my sister Michelle, for their concern over the years. My attendance at MIT probably meant more to them than it did to me. Being able to study in America would have been impossible without the dedication and trust from my parents.

Most importantly, I want to thank God for being with me and keeping me strong in faith throughout the whole process.

The work for this thesis was carried out in the Summer and Fall semester of 1993 at Intel Corporation, Santa Clara, California as part of IIB intership program at MIT. This document was written in the Fall term of 1993 at Intel and was revised in the Spring term of 1994 at MIT.

Table of Contents

Abstract.....	2
Acknowledgement	3
1. INTRODUCTION	10
2. BACKGROUND	12
2.1. Motivation	12
2.2. Methods of the bumping process in C4.....	18
2.3. Materials Selection.....	25
2.4. Growth Kinetics and Order of Reactions - An Overview.....	25
2.5. Electrochemical Principles of Pb/Sn Solders.....	29
3. EXPERIMENTAL PROCEDURES AND METHODS	31
3.1. Thickness Morphology and Composition of the Surface Layer of Solder Bumps.....	31
3.2. Gravimetric Test of Pb Compounds	35
3.3. BLM Layer Etch Rate Study	36
4. RESULTS AND DISCUSSION.....	37
4.1. Thickness Morphology and Composition of the Surface Layer of Solder Bumps.....	37
4.2. Gravimetric Test.....	47
4.3. Reaction Mechanism for Surface layer growth studies of Solder Bumps.....	51
4.4. BLM Layer Etch Rate Studies.....	61
5. CONCLUSIONS AND RECOMMENDATIONS.....	67

5.1. Conclusions.....	67
5.2. Recommendations.....	70
APPENDIX I. Binding Energy of Pb compounds.....	71
APPENDIX II. XPS Results of Pb Compounds.....	74
APPENDIX III. Thermodynamic Properties of Pb Compounds.....	77
REFERENCES.....	78

LIST OF FIGURES

Figure 2.1. Flip Chip	12
Figure 2.2. Self-Alignment of Flip Chip.....	13
Figure 2.3. Experimental Energy vs. Shear Displacement.....	14
Figure 2.4. Tape Automated Bonding (TAB)	15
Figure 2.5. IBM Thermal Conduction Module	16
Figure 2.6. A schematic Diagram of C4 bumps	19
Figure 2.7. Solder Bump Structures and procedures.....	20
Figure 2.8. BLM layers of C4 bumps	21
Figure 2.9. Study on height of the bumps after reflow.....	22
Figure 2.10. Wet Etch technique for removal of BLM layers.....	23
Figure 2.11. Lift off technique for removal of BLM layers.....	24
Figure 2.12. Growth rate in the transformation of beta tin to alpha tin.....	26
Figure 2.13. Growth by diffusion.....	27
Figure 3.1. Electroplating Process.....	32
Figure 4.1. The surface of Pb/Sn Solder bumps after high sulfuric concentration bath.....	39
Figure 4.2. The surface of Pb/Sn Soder Bumps after high sulfuric concentration bath.....	39
Figure 4.3. The surface of Pb/Sn solder bumps after low sulfuric concentration bath.....	40
Figure 4.4. 2000X Magnification.....	40
Figure 4.5. Soder Bumps before BLM etch.....	41
Figure 4.6. Solder Bumps before BLM etch.....	41

Figure 4.7. Solder bumps after BLM etch.....	42
Figure 4.8. Solder bumps after BLM etch.....	42
Figure 4.9. Solder bumps after acid cleaning and after reflow.....	43
Figure 4.10. Solder bumps after acid cleaning and after reflow.....	43
Figure 4.11. XPS scan on the cross section of Pb/Sn plated wafer after 86% H ₂ SO ₄ Bath.....	46
Figure 4.12. The trend of solubility of PbO in the Pourbaix Diagram for Pb Comounds.....	48
Figure 4.13. Growth of Surface Layer vs. Concentration of H ₂ O ₂ (4 min. etch)	52
Figure 4.14. Growth of Surface Layer vs. Concentration of Sulfuric Acid (4 min. etch).....	52
Figure 4.15. Cross Section of Pb/Sn solder bumps after 90% H ₂ O ₂ bath (4 min. etch).....	54
Figure 4.16. Cross section of Pb/Sn solder bumps after 100% H ₂ O ₂ bath (4 min. etch).....	54
Figure 4.17. Cross section of Pb/Sn solder bumps after 100% H ₂ SO ₄ bath (4 min. etch).....	55
Figure 4.18. Cross section of Pb/Sn solder bumps after 33% H ₂ SO ₄ bath (4 min. etch).....	55
Figure 4.19. Cross section of Pb/Sn solder bumps after 50% H ₂ SO ₄ bath (4 min. etch).....	56
Figure 4.20. Cross section of Pb/Sn solder bumps after 66% H ₂ SO ₄ bath (4 min. etch).....	56
Figure 4.21. Cross section of Pb/Sn solder bumps after 80% H ₂ SO ₄ bath (4 min. etch).....	57
Figure 4.22. Cross section of Pb/Sn solder bumps after 86% H ₂ SO ₄ bath (4 min. etch).....	57
Figure 4.23. Cross section of Pb/Sn solder bumps after 91% H ₂ SO ₄ bath (4 min. etch).....	58

Figure 4.24. Cross section of Pb/Sn solder bumps after 100% H₂SO₄ bath (4 min. etch)..... 58

Figure 4.25. Growth of surface layer vs. etch time in peroxide-rich concentration..... 59

Figure 4.26. Growth of Surface layer vs. (etch time)^{1/2} in H₂SO₄-rich concentration.....59

Figure 4.27. Diagram of BLM layer in a lateral and vertical direction..... 62

Figure 4.28. The undercut of BLM layer after 86% H₂SO₄ for 1 min. 62

Figure 4.29. The undercut of BLM layer after 86% H₂SO₄ for 3 min. 63

Figure 4.30. BLM layer Undercut Etch..... 64

Figure 4.31. BLM layer Vertical Etch..... 64

LIST OF TABLES

Table 4.1. Percentage composition of Surface analysis using AES.....	38
Table 4.2. Percentage composition of Surface analysis using XPS.....	44
Table 4.3. Binding Energy of Pb oxides using NIST data.....	44
Table 4.4. Gravimetric test results for Pb oxides.....	49
Table 4.5. Solubility of PbO.....	50

CHAPTER 1. INTRODUCTION

With recent advances in silicon technology, microprocessor performance is becoming limited by chip-to-package interconnections. The three primary assembly processes are: Wirebonding (WB), Tape Automated Bonding (TAB), and Controlled Collapsed Chip Connection (C4). Wirebonding is a method where semiconductor components are attached with very fine wire. These components interconnect with each other or with a package lead. TAB is the process to join silicon chips to patterned metal on polymer tape and then attaching silicon chips to a substrate or board by outer lead bonding [Tummala and Rymaszewski, 1989, pp. 1151-1154].

C4 is a technology where a chip is interconnected to a package by a matrix of solder bumps. This solder-bump interconnection was originated by IBM in the early 1960s to remove several problems of manual wirebonding, such as low productivity, high expense and unreliability due to mechanical connectors. TAB also has several disadvantages over C4, such as total input/output count limited by pitch, the high cost of high performance TAB tape and the complexity of the total process. C4 has several potential advantages over TAB and WB. First, C4 offers a high input/output density by placing solder bumps anywhere on the chip in an array. Second, interconnection by very small solder bumps lowers inductance, this enhancing the overall electrical performance. Finally, C4 allows for lower process complexity due to the relaxation of pitch requirements and the self-aligning property of C4 die attach.

This study focuses on C4 solder bumps to understand Pb/Sn surface layer formation kinetics, as well as analysis of layer composition and morphology of C4 bumps after base metal etch. In addition, the effect of using etchants for removing the surface layer to improve the solderability of solder bumps, and the etch rates of Ball Limiting Metallurgy (BLM) layer and its etch mechanism were studied.

Specifically, C4 was studied from three view points. First, the kinetics of reaction of the surface layer with sulfuric acid and H_2O_2 etch were studied in depth. The thickness variation of the surface layer as well as its composition caused by the interaction of H_2O_2 and sulfuric acid was studied by the rate of growth of the surface layer as a function of time. A model was developed to examine the rate limiting step in the formation of these layers. The composition and morphology of those layers were also analyzed using XPS, AES and SEM. Moreover, solubility testing was performed to confirm the spectroscopy data results. From these data, the optimal etchant composition which results in the thinnest surface layer and most efficient etch of BLM layer, and its etch time was determined.

Second, removing the surface layer before reflow, using the right acid, is the most important step for good reflow and durability of solder bumps. The selection of acid can be determined using electrochemical principles of Pb/Sn solders and using the Pourbaix diagram of Pb compounds as explained in Section 2.4. The pH change of this acid was studied extensively and the solubility of the surface layer was observed.

Finally, the BLM layer etch rate in the lateral and vertical directions was studied to determine optimal etchant composition. Forming a thin layer on the surface using the correct composition of etchant is important, but it is equally important that the current composition completely etches the BLM layer around bumps after plating. SEM was used to take pictures of cross sections of bumps. The thermodynamics and kinetics of the etch rate will be discussed.

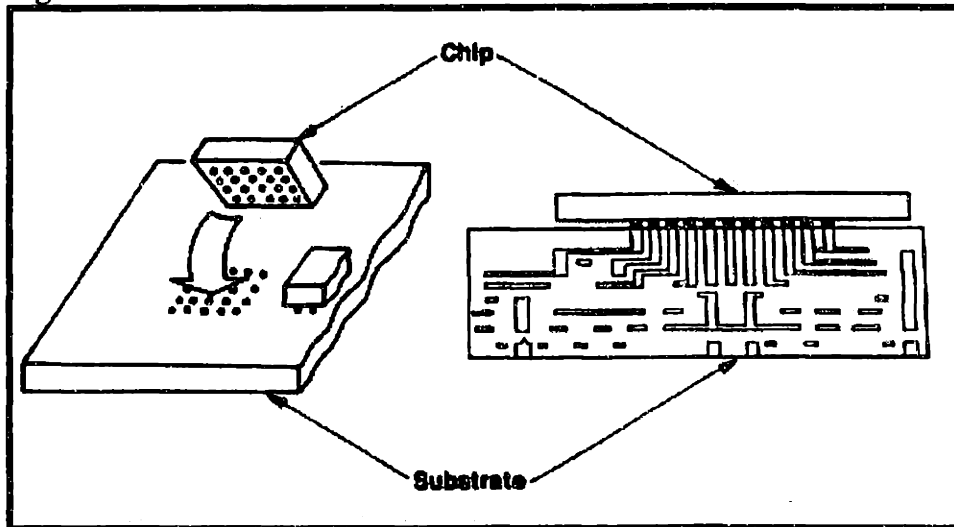
CHAPTER 2. BACKGROUND

2.1. Motivation

C4 Technology is important for chip-to-package interconnections and offers many advantages over TAB and WB. One advantage is the high input/output density of the C4 process, which enables bumps to be placed anywhere on the chip so that it is easier to make connections to the circuitry at those points [Jackson et. al., 1991, pp. 82-85]. Short solder bumps improve overall electrical performance and allow more control of the size of the chip. Moreover, the higher density of I/O per chip allows a higher degree of integration at the first packaging level than ones with edge-connect packages, such as WB or TAB.

C4 technology is also referred to as "Flip Chip" because the chip is self-aligned

Figure 2.1.

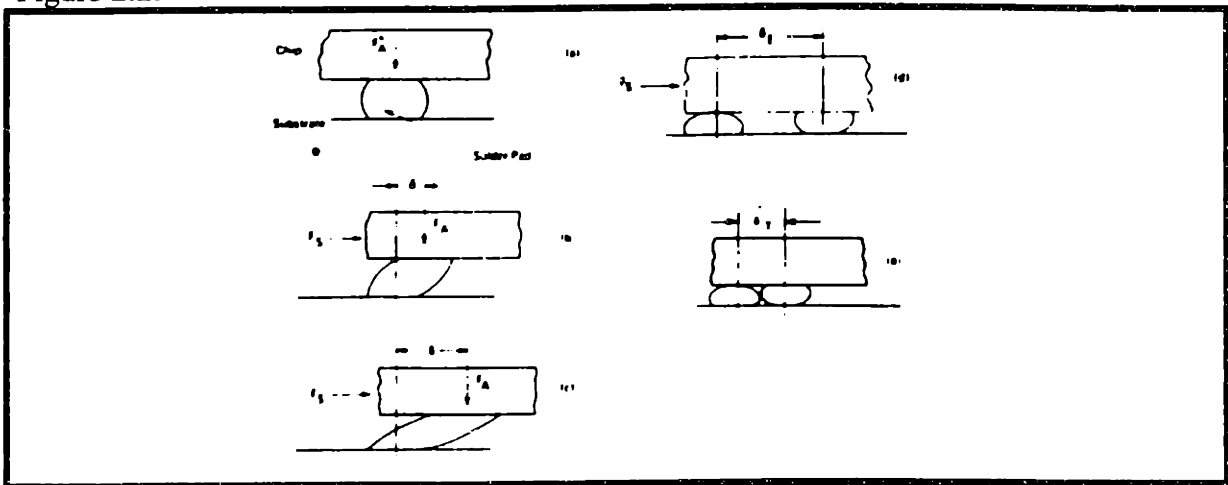


[source: Tumala et. al., 1989, pp.366]

to the substrate (upside-down) and the surface tension of solder allows solder balls to form self-aligned metallurgical joints with the substrate as shown in Figure 2.1. The self-alignment feature allows high yields even when dealing with chips with very high pin

counts. During chip joining, self-alignment automatically corrects relatively coarse chip placement during solder reflow. This is not possible for TAB or WB. Studies done by Goldman et. al. (1972) demonstrated self-alignment capability of a flip chip. These studies showed that within a certain limit, a misaligned chip self-aligns during reflow joining. The mechanical energy of a molten solder pad is made up of gravitational and surface energy, the joint always having the shape which minimizes total energy. Gravitational energy being negligible, for small balls (less than 1 mm in size), free surface area can then be viewed as a direct measure of the pad energy. Goldman discovered that the minimum distance of critical energy or touching is the maximum center-to-center mis-registration δ_R which can be realigned as shown in Figure 2.2:

Figure 2.2.



[source: Goldmann, 1972, pp.333]

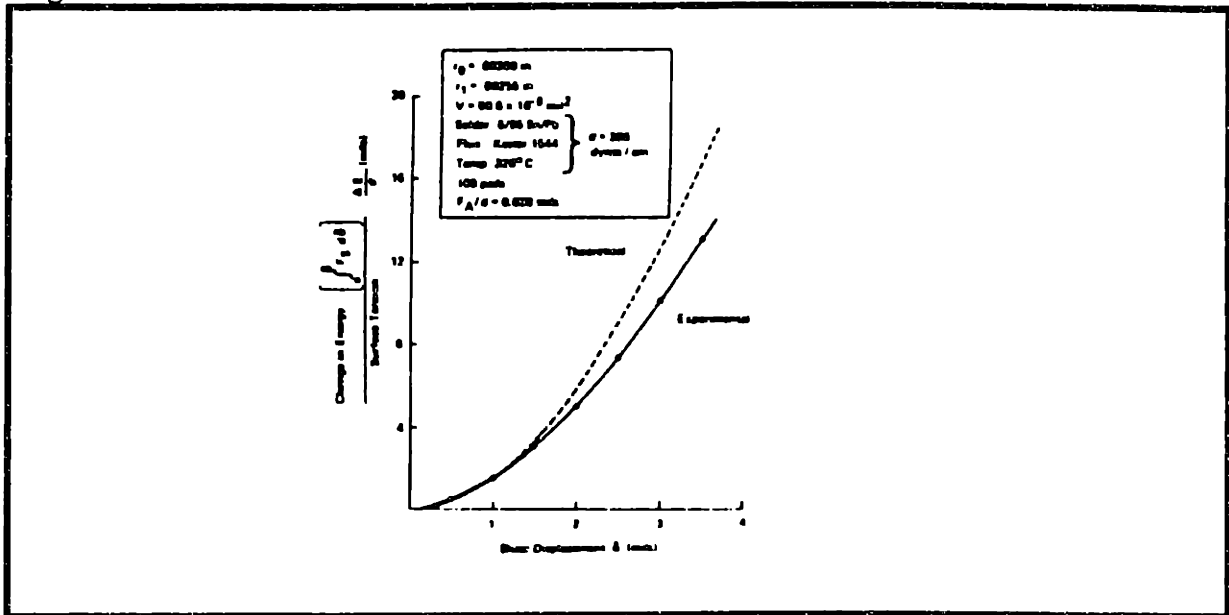
$$\delta_R = \min (\delta_E, \delta_T).$$

where δ_E is the minimum critical energy distance and δ_T is the touching distance.

Goldman proved that for small displacements, the energy is close to his predicted value, but the experimental energy is increasingly less than the theoretical value for larger

displacements (Figure 2.3). Therefore, the degrees of misregistration that can be re-aligned in solder-reflow chip joining is limited by the touching distance. Also,

Figure 2.3



[source: Goldman, 1972, pp.336]

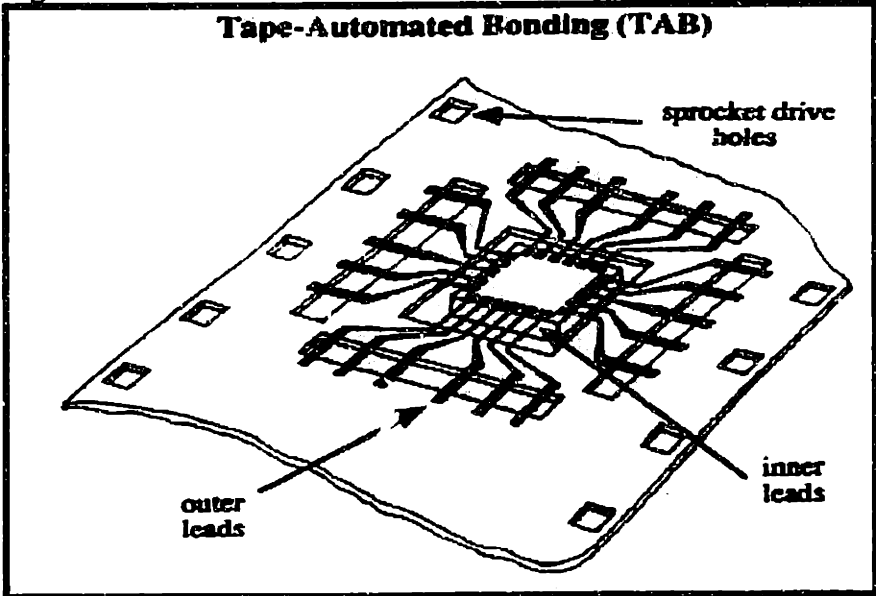
Goldman showed that a pad of interface radius (R) can have a center-to-center offset of at least the touching distance or three times the average interface radius [Goldman, 1972, pp.332-339].

TAB processes use thermocompression bonding to attach silicon chip pads to patterned metal on polymer tape (Figure 2.4). This process is known as inner lead bonding (ILB). Following ILB, the chip is then encapsulated or tested. The individual die is subsequently removed from the tape and packaged using outer lead bonding (OLB) techniques.

The C4 process costs less than TAB and WB because of the bumping process, the simplified assembly processes and the improved cost performance ratio for C4 packages. The bumping process takes place instantaneously; whereas, WB makes each connection

from chip to package through a manual or automatic set of routes with wires. The cost of equipment, maintenance and downtime of C4 is lower because of its self-alignment capability; the greater the misalignment that can be corrected, the less accurate chip placement would be needed [Goldman, 1972, pp.332-339].

Figure 2.4.

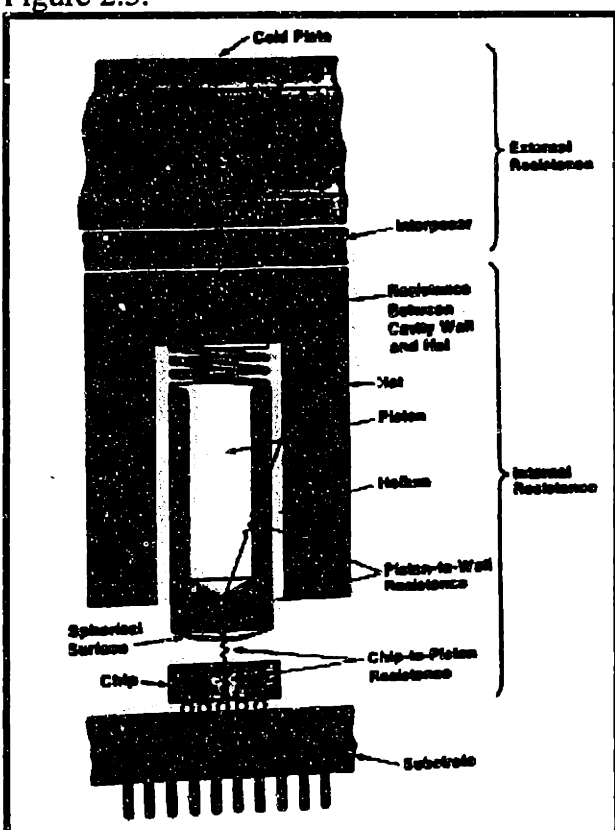


[source: Charles, 1989, p. 233]

Flip chips have more thermal advantages relative to back bonding where the package is placed on the top of the chip. In the past, a constraint with flip-chip bonding was the poor dissipation capability compared to backside bonding. Area array bumps, compared to peripheral bumps, resulted in an increase in heat dissipation because area array bumps increased the number of joints and their greater closeness to the device. Heat dissipation is a crucial factor in flip-chip bonding because of a device's ability to eliminate heat greatly affects the maximum power capability. However, since the back of the flip-chip is mechanically and electrically free of delicate surface features, flip-chips are now competitive thermally with back-bonding by having a variety of heat sinks on the back of a chip. For example, the IBM Thermal Conduction Module, TCM (Figure

2.5), can dissipate 4 watts per chip and up to 300 watts for a 100 or a 118-chip module. This system has spring-loaded pistons transferring heat from the back of each chip to a water-cooled plate attaching a solder joint thermal path [Goldmann & Totta, 1983, pp. 91-97]. As an enhanced conduction path, Helium gas encapsulation has been developed for this conduction cooling machine because of its high thermal conductivity [Oktyay & Kammerer, 1982, pp. 55-66].

Figure 2.5.



[source: Goldmann & Totta, 1983, pp. 94]

This cooling and encapsulation concept depends on the used of spring-loaded “pistons” in contact with each chip. R.C. Chu et. al. (1982), did further studies on TCM modules and established that the TCM cooling concept is thermally superior to its Liquid-Encapsulated Module (LEM) predecessor. D.M. Cavanaugh (1975) compared flip-chip

thermally with wire-bonding. Two chip/substrate package configurations were tested for θ_{j-a} , θ_{j-s} and maximum power dissipation; one to study flip chip reflow die attachment and one to study chip-to-wire attachment. Here, θ is a thermal resistance factor, defined as:

$$\theta = \Delta T / P \quad ^\circ\text{C} / \text{Watt}$$

where P = power and $\Delta T = T_j - T_0$ where T_j = Device Junction temperature and T_0 = temperature of heat sink or ambient if the atmosphere is the ultimate heat sink. Also, θ_{j-a} , θ_{j-s} stand for Thermal resistance from junction to ambient, from junction to substrate respectively. As a result, thermal resistance of the mounted flip was higher when compared to a chip- and-wire configuration. These advantages enabled us to choose C4 over TAB or WB.

Myers (1969) gave an overview of flip-chip die bonding. The potential advantages of IC flip-chip bonding are to eliminate wirebonds, to reduce assembly costs, and to improve reliability. Packaging costs are as much as 80% higher for wirebonds since each wire has to be bonded individually. The flip chip reduces the failures and costs associated with wirebonding. Also, the substrate materials along with the substrate interconnect pattern provide mechanical supports and act as a heat sink. The substrate-to-conductor pattern interface metal serves as a thin film resistor in hybrid applications. Moreover, the metallurgical system between the silicon chip and the substrate used for the chip interconnection pattern-the bump, the substrate interconnection pattern, and interfacing and bonding between them- is the single most important variable in flip chip. These interfacing materials are required to improve mechanical adhesion and to join two noncompatible metals. Also, this bonding method provides joining between the bump and the conductor pattern, as well as, high strength and low resistance bond at low costs. Solder bonding offers several advantages such as lower temperature processing above the temperature of the molten solder required, rework capability and the simple soldering process [Myers, 1969, pp.131-144].

2.2. Methods of the bumping process in C4

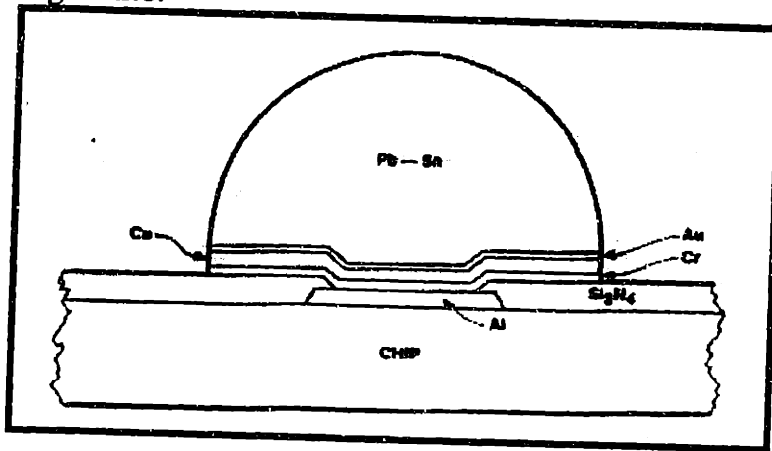
There are two types of solder bump formation for Flip Chip Technology: evaporation and electroplating. In this chapter, these two processes and their advantages and disadvantages are discussed.

Flip chip technology was originally developed at IBM in the 1960s to resolve problems involving manual wirebonding. After passivation patterning, the under-bump-metallization (UBM), such as chromium/copper/gold layers are sequentially deposited through holes of a metal mask using an evaporator. Chromium acts as an adhesion promoter and diffusion barrier metal layer which makes contact with Al-Si electrode pads. A layer of copper is then deposited, providing solder wettability. To prevent copper from oxidizing, a layer of gold is deposited above the copper layer. Finally, Pb/Sn solders are deposited sequentially through the same mask using another evaporator. These wafers are then placed in an H₂ ambient furnace at 365 °C for reflow to obtain spherical bump shape. The bumps melt and wet only at the Cr/Cu/Au areas. H₂ reduces minor Pb/Sn oxides. The surface tension of the bumps results in a spherical shape after reflow at about 365 °C. A schematic diagram of C4 bumps using the IBM method is shown in Figure 2.6. This evaporation method is performed in a vacuum. Because the deposition process is continuous and the key layers are blended together, layers do not need to be separated from one another. Although the IBM method is well established, costs associated with the deposition process are high. Moreover, due to differences in the thermal expansion coefficient between the Si wafer and metal mask, as wafer size increases, good dimensional accuracy of bumps is very hard to obtain [Tumala & Rymaszewski, 1989, pp.366].

An alternate method for depositing solder bumps is electroplating. Blanket layers of metal or Ball Limiting Metallurgy (BLM) are sputtered on the wafer. Electroplating is a deposition of metallic coating onto a conductive object placed in an electrolytic bath.

Using the terminal as the anode, a DC current is passed through the solution affecting transfer of metal ions onto the cathodic surface.

Figure 2.6.

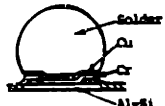
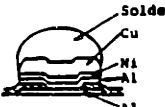
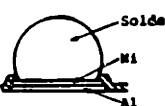

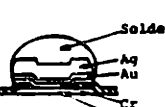
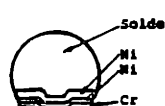



[source: Nagesh, 1982, pp.10]

In the case of C4, this is the BLM layer. Photoresist is then applied on the BLM film coated wafer and the resist is patterned using the photolithography process. The wafer is then subjected to electroplating and Pb/Sn bumps are formed in the open vias in the patterned resist. After stripping the resist, using the bumps as a mask, the thin film metal layers are selectively etched to electrically isolate the bumps from each other. The electroplating method requires the right selection of a base metal stack because the solder is soluble in almost every acid and is vulnerable to the etching solutions of the base metal [Tumala & Rymaszewski, 1989, pp.378]. During this etch process, thin layers are chemically formed on the surface of the Pb/Sn bumps. These layers impact the solderability of the solder bumps and must be removed. Although the electroplating method seems to be easier and a more economical bumping process than IBM's original "metal mask" vacuum deposition method, the etching of base metal stacks, without etching away plated solder bumps, has remained a difficult problem.

Several studies have been conducted to fabricate bumps by electroplating. Studies done by Kawanobe et.al. (1981) summarized the past solder bump fabrication processes produced by plating (Figure 2.7). One of the fabrication by electroplating

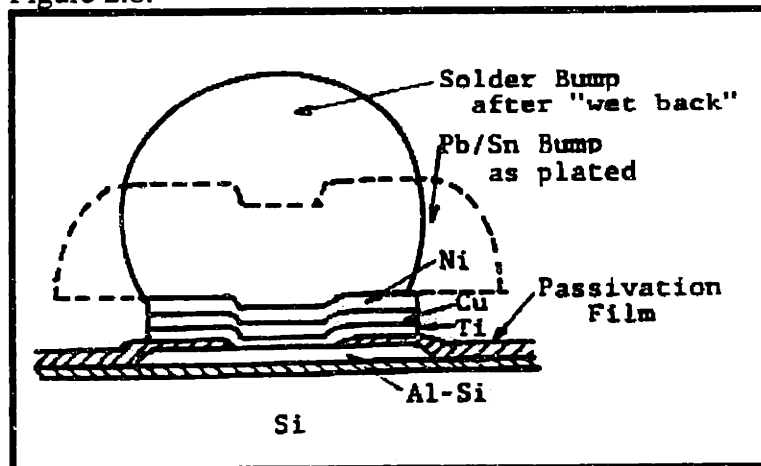
Figure 2.7. Solder Bump structures and procedures

Maker	Structure	Procedure	Notes
IBM		<ol style="list-style-type: none"> 1. Metal Mask Alignment 2. Au/Cu/Cr Deposition 3. Metal Mask Alignment 4. Sn-Pb Deposition 5. Wet Back 	"Controlled Collapse Interconnection" ref. (1)
Philips		<ol style="list-style-type: none"> 1. Ni/Al Deposition 2. Photoresist 3. Ni Etch 4. Photoresist 5. Sn-Pb/Cu Electro. Plate 6. Al Etch 7. Reflow 	"IC on Tape" ref. (3)
Sanken Electric		<ol style="list-style-type: none"> 1. Ni/Al Deposition 2. Photo-Etch 3. Passivation & Through-Hole 4. Metal Aperture Alignment 5. Sn-Pb Ball Placement 6. Reflow 	ref. (4)
"A"		<ol style="list-style-type: none"> 1. Ni/Al Deposition 2. Photoresist 3. Au/Ni Electro. Plate 4. Ni, Al Etch 5. Solder Dip 	Procedure is speculated from the structure.
"B"		<ol style="list-style-type: none"> 1. Au/Cr Deposition 2. Photoresist 3. Ag Electro. Plate 4. Au, Cr Etch 5. Solder Dip 	Procedure is speculated from the structure.
"C"		<ol style="list-style-type: none"> 1. Ni/Cr Deposition 2. Photoresist 3. Ni Etch 4. Photoresist 5. Sn/Ag/Ni Electro Plate 6. Cr Etch 7. Wet Back 	Procedure is speculated from the structure.
Philcoford		<ol style="list-style-type: none"> 1. Ni/Cr Deposition 2. Photoresist 3. Ni, Cr Etch 4. Ni Electroless Plate 5. Solder Dip 	Structure is speculated from the procedure. ref. (5)

[Source: Kawanobe et. al., 1981, pp.150]

methods was to make nickel or silver spacers but bumping by dip soldering made it very difficult to build up higher solder bumps. Also, as shown in Figure 2.7, this bumping process is done by an electroplating method, but supplying plating current through thin and high resistant films result in a large thickness distribution on a wafer. The method used by Philips was electroplating. A corrodable Al layer for BLM was used. Knowing that the solder is very vulnerable to etching solutions of BLM, Kawanobe et. al. finally selected a Cu layer for a solder wettability barrier against the reaction between Al and solder and for the conductive layer. A TiW layer was used as an adhesive with Pb/Sn solders (Figure 2.8). These layers were then etched off without attacking the solder using EDTA, H₂O₂ and H₂SO₄. Sn and Pb are plated separately to control only the Pb-Sn solder constitution. This study also determined the height of the bumps after reflow (Figure 2.9).

Figure 2.8.



[source: Kawanobe et. al. 1981, pp.149]

The relation between the height and the plating thickness is an important criteria in determining the bump height. The volume after plated V_1 is defined in the following:

$$V_1 = \pi \int [r + a/t \sqrt{t^2 - x^2}]^2 dx = \pi[r^2t + \pi/2 art + 2/3 a^2t]$$

The volume of bump after reflowed shape V_2 is:

$$V_2 = \pi \int [R^2 - x^2] dx \text{ where } R = h^2 + r^2 / 2h$$

$$= \pi/6 h[h^2 + 3r^2]$$

In practice, the volume difference between V_1 and V_2 can be expressed as:

$$V_2 = \alpha V_1$$

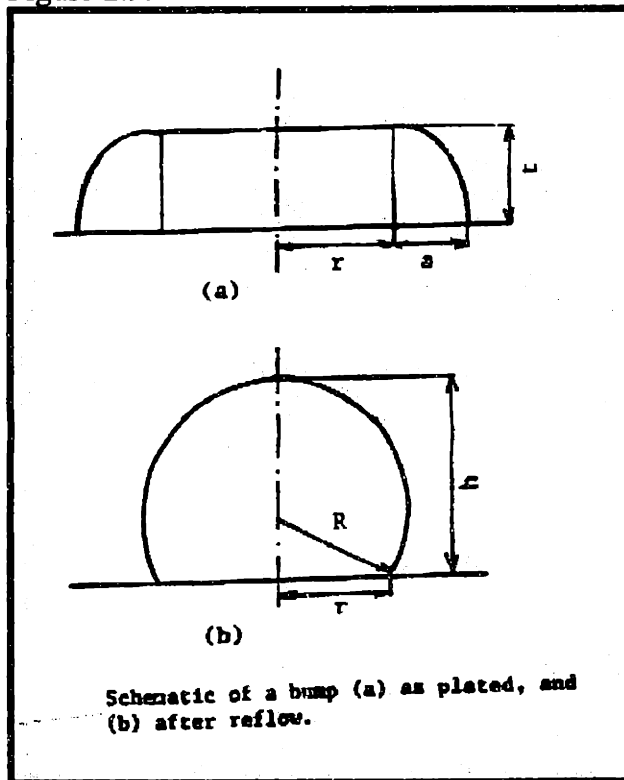
where α is a correction factor

$$h^3 + 3ph + 2q = 0$$

where $q = -3[r^2t + 1/2 \pi a r t + 2/3 a^2 t] \alpha$

$$p = r^2$$

Figure 2.9.



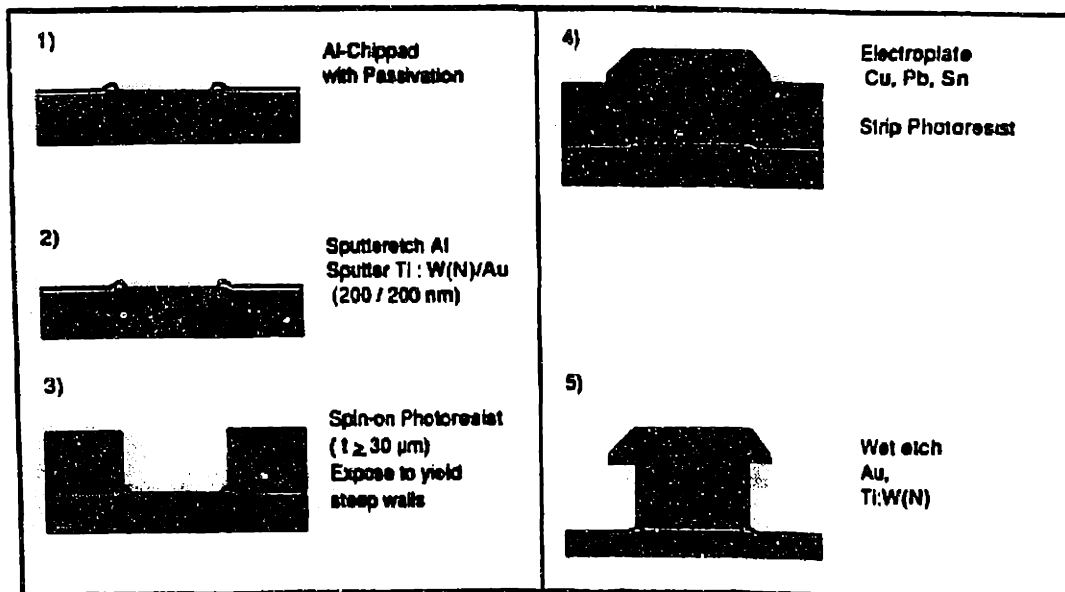
[source: Kawanobe et. al., 1981, pp. 152]

Then using the last two equations:

$$h = 3 \sqrt{-q} + \sqrt{q^2 + p^3} + 3\sqrt{-q} - \sqrt{q^2 + p^3}$$

This calculation concluded that bump height of 100 μm or more is necessary for controlled collapse solder interconnections. Also, approximately 50 μm or more "uniform thickness" is required after plating. This study showed that thickness uniformity distribution on a whole wafer depends on the current density, the flow rate of plating solution through the bath, and a cylindrical-shaped plating bath where a wafer and an anode are placed opposite to one another [Kawanobe et. al., 1981, pp.149-155]. Another study done by Wolf, J. et.al. (1993), demonstrated an electroplating method for the bumping process. Using TiW/Au /Cu BLM, Wolf achieved low processing costs and better resolution by two approaches of Pb/Sn solder bumping. In Figure 2.10, wet

Figure 2.10.



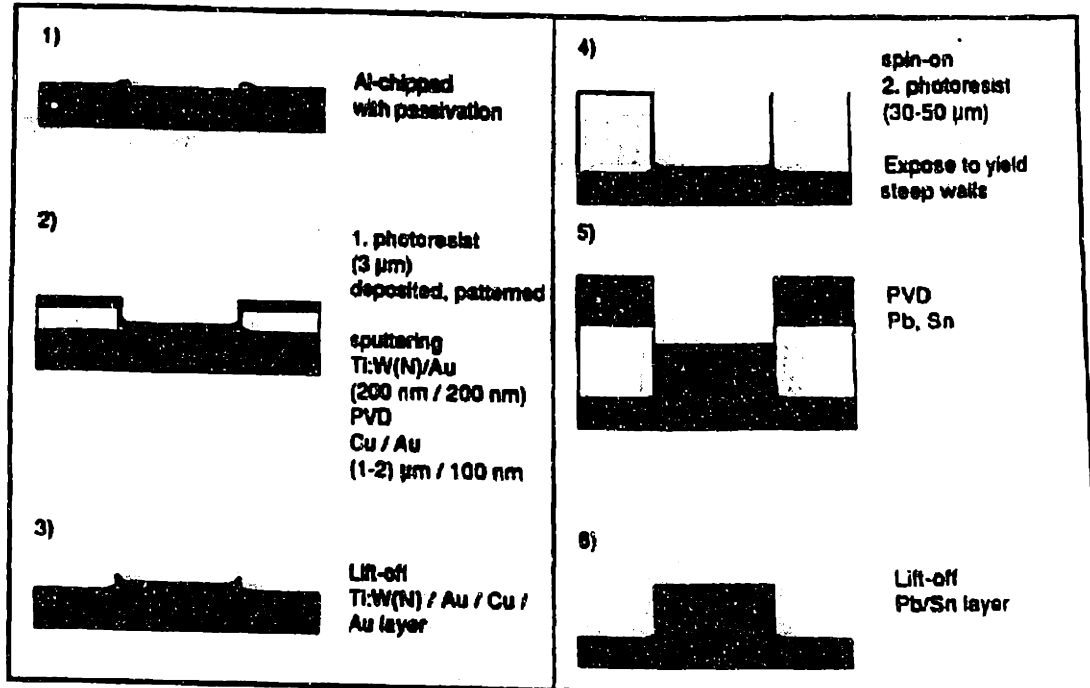
[source: Wolf et. al. 1993, pp. 143]

etch is used to remove BLM around solder bumps. Another method used is a lift off technique instead of wet etching steps. A lift off technique avoids wet etching steps by sputtering BLM layers onto a resist mask, followed by PVD of copper and also by a thick second photoresist layer to achieve PVD of lead and tin (Figure 2.11). Both methods

proved to be viable so that benefits of both techniques can be compared and used [Wolf et. al. 1993, pp. 141-152].

After these Pb/Sn solder bumps are plated, the BLM around the bumps is etched. Studies done by Kawanobe, T. et.al. (1981) indicated that a combination of hydrosulfuric acid and hydrogen peroxide etches the BLM layer. Combination of Sulfuric acid and H₂O₂ are used to etch the base metal layer in this project. These acids create sulfur containing oxide layers on the surface of the bumps. These oxide layers on the surface serve as protection layers and as masks against other BLM etchants. After the base metal layer etch is applied, these oxide layers on the surface need to be eliminated from the bumps to allow for solderability of bumps during reflow.

Figure 2.11.



[source: Wolf et. al. 1993, pp. 146]

2.3. Materials Selection

There are several reasons why Pb/Sn solders are chosen over other combinations of solders such as Pb/In, In/Sn and Cu/Pb. First, high-lead composition solder (97% Pb and 3% Sn) was selected because its melting point is about 315 °C, which prevents C4 bumps from remelting at the package-to-board level of assembly. Wafers are then placed in an hydrogen furnace at 360 °C for reflow [Tumala & Rymaszewski, 1989 pp.369]. The choice of BLM is important for these solders because these layers have to be good conductors for plating, minimizing the formation of intermetallics with Sn and forming a good protection layer for better adhesion and uniform plating. Studies done by Bowlby at Motorola, indicated that Pb/Sn solder bumps ranging from 60/40 to 95/5 are preferred for the following reasons: improving storage and aging characteristics, and wetting characteristics of solder bumps.

2.4. Growth Kinetics and Order of Reactions - An Overview

Since the growth kinetics of surface layer on Pb/Sn bumps was examined in this study, its overview is explained. Growth kinetics becomes important after the undeveloped embryo has exceeded a critical size and become a stable nucleus. The rate at which heat of fusion is removed largely controls the growth rate of new phase during solidification. Considering simple growth, where a new phase growing from another phase by simple transfer of atoms of a single component, an equation shown below describes the net rate of atom transfer from the matrix to a particle (being equal to the difference in the rate of atom movement toward and away from the particle) :

$$I = S\nu e^{-\Delta g_a/kt} (1 - e^{-\Delta g\beta\alpha/kt})$$

Where S = number of atoms facing the surface, ν = an atomic vibration frequency

I = net number of atoms per second leaving the matrix to join the beta phase

α = matrix phase, β = embryo phase.

Assuming that when the atoms jump, they move through an average distance λ . The velocity of the boundary will be given by:

$$v = \lambda I / S$$

Where I/S = the average number of per atoms' jumps per second facing the boundary

λ = the distance corresponding to each of these jumps.

Assuming $\Delta g_{\alpha\beta} \ll kT$ for a sufficiently small supercooling, the growth velocity becomes:

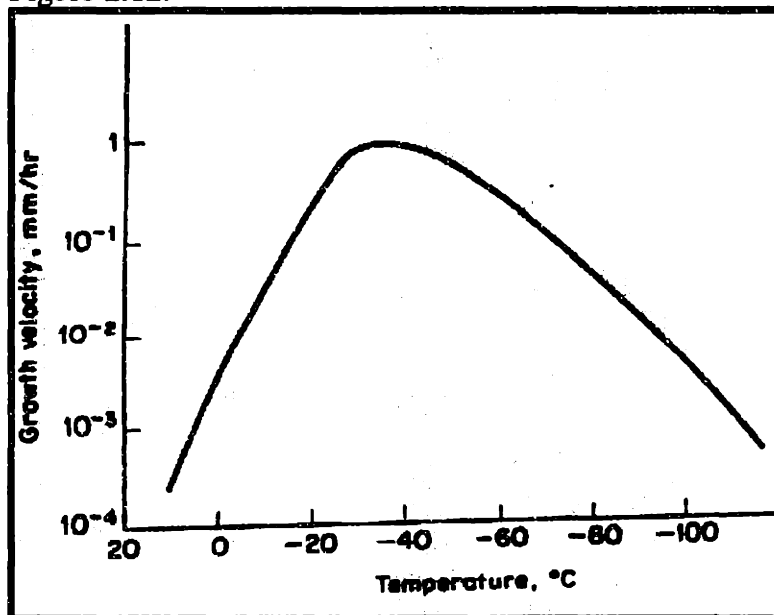
$$v \approx \lambda v (\Delta g_{\alpha\beta}/kT) \exp(-\Delta g_{\alpha}/kT)$$

For a large degree of supercooling, the velocity equation may be written as:

$$v \approx \lambda v \exp(-\Delta g_{\alpha}/kT)$$

Figure 2.12 shows this growth rate in the transformation of beta tin to alpha tin [Reed-Hill and Abbaschian, 1973, pp. 498-501].

Figure 2.12.

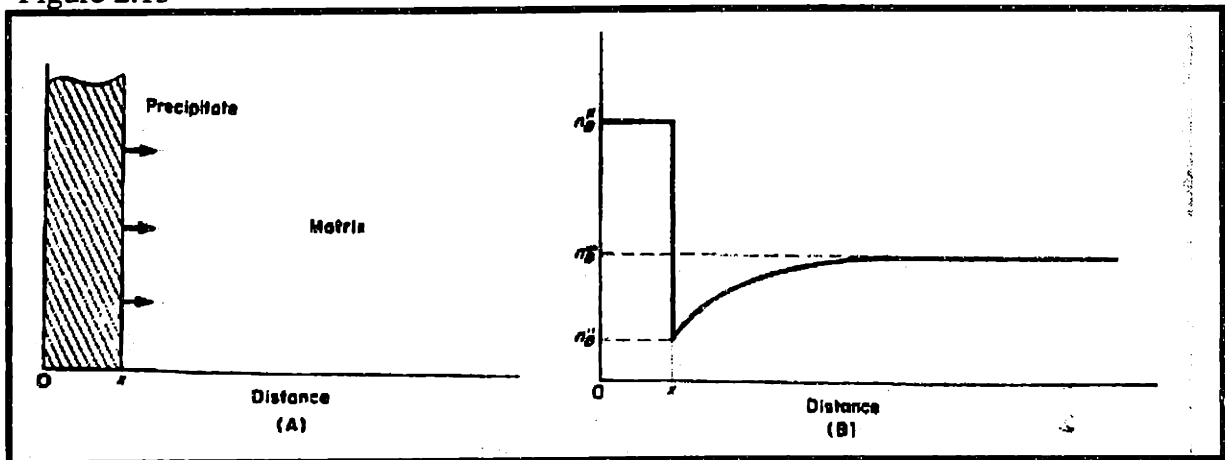


[source: Reed-Hill and Abbaschian, 1973, pp.501]

There is another type of growth where formation of a new phase occurs that is different from the composition of old phase. As shown in Figure 2.13, the growth is controlled by diffusion. According to Zener's theory, whenever, the growth is controlled by a simple diffusion process, the interface position varies with the square root of time and the growth velocity varies inversely as the square root of time.

$$x = a^* \sqrt{Dt}$$

Figure 2.13



[source: Reed-Hill and Abbaschian, 1973, pp.502]

where x = thickness layer growth, D = diffusion coefficients and a^* = parameter for dimensional growth. So if the reaction rate of two molecules forming growth is fast enough, then diffusion is the rate-limiting step. Otherwise, the growth rate can be controlled by the chemical reaction rate, where growth of thickness is directly proportional to time,

$$x = c t \quad \text{where } c = \text{a constant}$$

Therefore, the rate of surface oxide layer growth in this study can determine the rate-limiting step. To determine the order of the reaction, the concentration of H_2SO_4 and H_2O_2 was varied as well since the rate-controlling step is determined by both

concentration and time for those acids which react with Pb/Sn solders [Reed-Hill and Abbaschian, 1973, pp.501-506].

2.5. Electrochemical Principles of Pb/Sn Solders

As mentioned earlier, removing the oxide layer on the surface of bumps is the most important step for reflow. The selection of acids can be explained by the Pourbaix diagram of Pb compounds which uses the relationship between electrode potential and pH equilibrium to show the region where the oxides are dissolved in aqueous solutions. Electrochemical reactions are different from chemical reactions in that an electrochemical reaction, instead of a chemical reaction, occurs at the interface between the metal and a solution of electrolyte. This interface enables us to measure the affinity of the reaction in magnitude and sign by the electrode potential. If the two potentials-- electrode potential E and equilibrium potential E_0 -- are equal, the affinity is zero and the thermodynamic equilibrium state of the reaction is obtained; if the electrode potential is above the equilibrium potential, the affinity is positive and the reaction can take place only in the direction of oxidation. However, if the electrode potential is below the equilibrium potential, the affinity is negative and the reduction reaction is only the reaction that takes place. The electrode potentials and pH are the characteristics of a metal/solution interface, where the metal or solution is the site of electric currents or chemical changes [Pourbaix, 1974, pp. 53-55].

When a metallic electrode is placed into a solution containing ions of that metal, an equilibrium is established between the trend of the metal to enter solution as ions (1), and the opposing force for the ions to lose their charge and deposit on the metal (2):



For this equilibrium to be established, a charge separation will occur to determine whether ionization or deposition happens faster. In other words, faster ionization will result by metal becoming negatively charged relative to the solution and faster deposition will result by metal becoming positively charged relative to the solution. Such a resultant potential, between the metal and the solution, is called electrode potential. Here,

the Nernst equation is given to measure the magnitude of the potential between a metal and a solution of its ions:

$$E = E_0 + (0.059/n) \log a$$

where E_0 is a constant characteristic of the material of the electrode, n =valence charge and a = activity of the metal ion [Lowenheim, 1978, pp.16-19] . Therefore, using these two characteristics, pH and Electrode potentials, a Pourbaix diagram of Pb compounds tells us to predict at which potential and pH of solution certain oxides can be dissolved as well as concentration of those oxides that have dissolved in a certain region. An example of a Pourbaix diagram is shown in the Results section of this thesis.

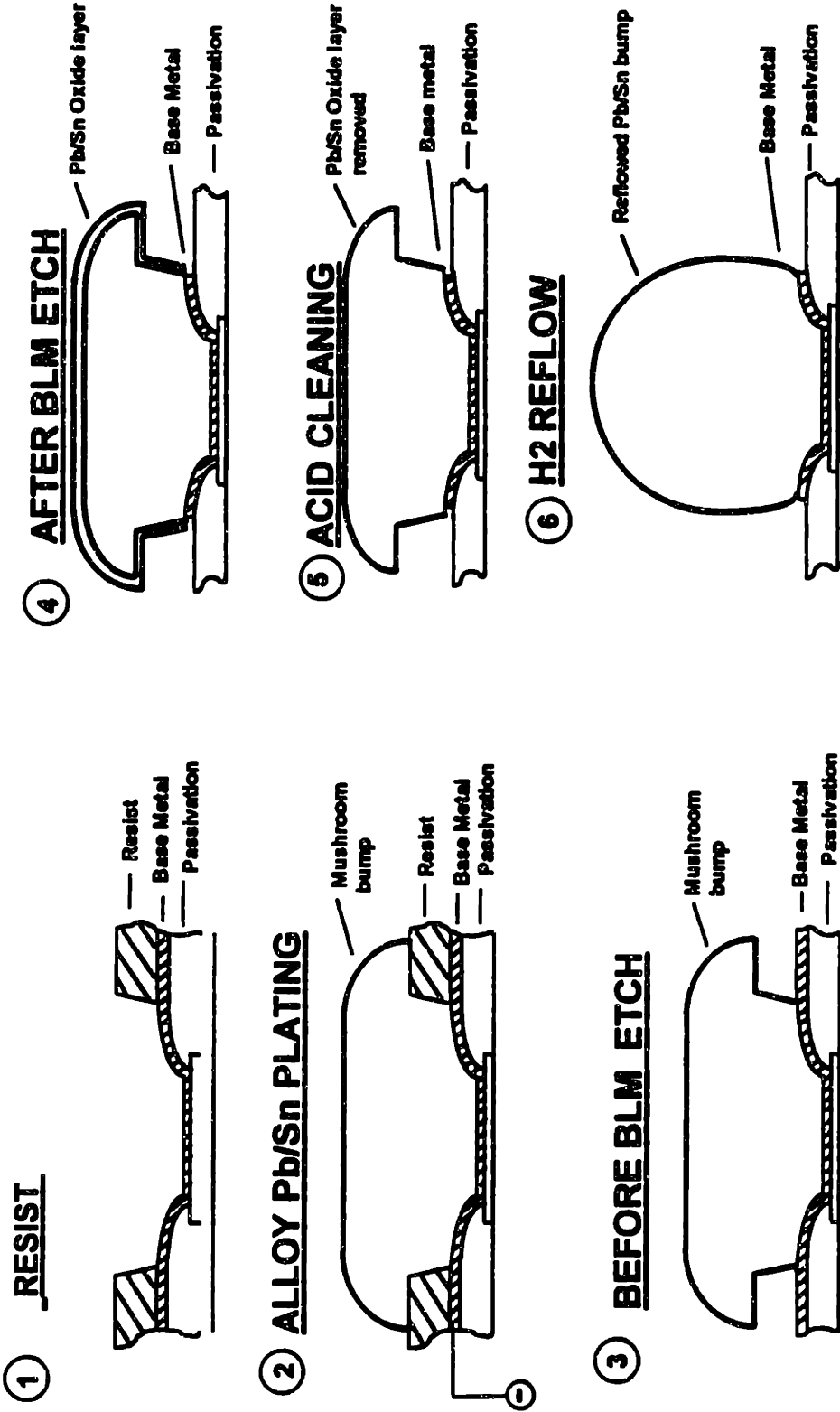
CHAPTER 3. EXPERIMENTAL PROCEDURES AND METHODS

3.1. Thickness Morphology and Composition of the Surface Layer of Solder Bumps

To prepare a sample for the morphology and composition studies, the process for bumping by electroplating is described. Blanket layers of metal or Ball Limiting Metallurgy (BLM) were deposited by Physical Vapor Deposition (PVD) on the wafer. Photoresist was then applied and patterned on the wafer using photolithography. The wafer was then subjected to electroplating of Pb/Sn bumps which were formed in areas not covered by resist as shown in Figure 3.1. After the plated wafer was prepared, the wafer was cut into dice to perform the experiments for the morphology and composition studies. The BLM etch bath of H_2O_2 and H_2SO_4 was prepared; the dice with Pb/Sn soldered bumps were put in the bath and were agitated to etch the BLM layer; During the etch, a surface oxide layer was formed on the bump. The size of the etch bath was about eight gallons. The concentration of H_2O_2 and H_2SO_4 was varied as well as the etch time to study the surface layer as a function of concentration variation in BLM etchant. Scanning Electron Microscopy (SEM) was used to study the thickness, the morphology of the surface layer and the etch rates of BLM layer.

Standard precision cross-section SEM technique which showed the cross section of Pb/Sn bumps, was performed. After the dice were exposed to various etchant baths, each die was cut into 4 small pieces with a scribe. A mixture of hardener and resin was prepared for an epoxyresin and a drop of this mixture was applied to a cover glass. This cover glass with the epoxyresin was then placed on the top of the die. A sample holder was used to hold the die and the cover glass together, and this sample was heated on a hot plate till the color of the epoxyresin changed to an amber color, and the epoxyresin hardened between the cover glass and the die. Then the sample was polished and mounted to grind the corner of the die using SiC grit papers with a roughness ranging

Figure 3.1. Electroplating process.



from 400-1200 sequentially. Top view optical microscopy was used to stop polishing once the center of the bumps was reached. Then, alumina oxide papers with a grain size ranging from 12 μm to 0.3 μm were used successively for final polishing. Since the Pb/Sn solder bumps were very soft and were easily oxidized, they require very careful polishing. The microscope was used to observe the cross section throughout this polishing process. After making a cross section of the sample, it was put in a gold sputter system to produce a few angstroms of Au which would prevent charging when using the SEM. Finally, the morphology and thickness of the surface layers of the bumps were studied using SEM.

After those samples were prepared, several spectroscopic techniques were used to analyze the surface of the solder bumps. The spectroscopic techniques had several limitations. Auger Electron Spectroscopy (AES) is the energy analysis of Auger electrons produced when an excited atom relaxes after ionization by a high-energy electron [Wolf, S. and Tauber, R.N., 1986, pp. 604]. Auger Analysis was used because it is surface-sensitive with typical analysis depth of less than 50Å, has a very small analysis area (5-10 μm) and can detect very small elemental concentrations on the surface, about 0.1 atom %. However, AES does not give any information about the bonding state of the elements.

X-ray Photoemission Spectroscopy (XPS) uses low energy x-rays, such as the K-alpha line of aluminum to cause photoelectron emission. The emission of photoelectrons is different from Auger emission in that XPS analyzes the electron that is "knocked out" of the atom. This equipment was used because it is surface-sensitive like AES and shows information about the bonding state of the elements. The limitation with XPS is that the difference in binding energy between Pb^{2+} and Pb^{4+} is less than 1 eV (Appendix I). In addition, the charging effect causes peak shifts which make it harder to distinguish to which peak the surface layer corresponds.

Secondary Ion Mass Spectrometry (SIMS) uses a medium energy beam of primary ions to sputter a sample. The intensity and mass of the secondary ions can be

used to determine the elemental composition of a sample. This equipment has a very high sensitivity and most elements can be detected. However the surface of the solder bumps was too rough to obtain accurate depth profiling. Furthermore, SIMS uses O_2^+ primary ions to sputter a sample. The molecular weight of the O_2^+ primary ion is same as the molecular weight for S which can not be detected, and the other primary ions, such as Cs^+ , required a very large spot size.

Energy Dispersive X-ray (EDX) was also used as EDX can detect elements with a thickness of more than 1 μm without sputtering by looking at a polished cross section of the bumps, gives a bulk concentration of the elements and gives a visual image of the sample using SEM. EDX is used in conjunction with SEM and does not require sputtering a sample. However, EDX has limited ability to distinguish between two adjacent X-ray peaks. The Pb peak is very broad and overlaps the S peak. So Pb and S peaks cannot be distinguished.

X-ray Fluorescence (XRF) was used to detect the elements present by using an X-ray source to irradiate the sample with high-energy photons. However, this equipment is able to detect elements starting from Na (atomic number of 11) so that the lighter elements, such as O, can not be detected.

Atomic Force Microscopy (AFM) was used to measure the grain size of the surface, but the surface of the layer was too rough to get a stable image.

Rutherford Backscattering Spectrometry (RBS) was used as it gives information on both the composition and depth distribution of elements by the energy of the backscattered ions. After an energetic beam of He ions impinges on the target, the He ions backscatter from the near surface region of the sample and are collected by a solid state detector. The limitations with this equipment are the poor spatial resolution (1 mm) and low detection limits for low atomic number elements. Moreover, the surface of the layer was too rough to obtain accurate depth distribution of the elements [Wolf, S. and Tauber, R.N., 1986, pp. 604-611]. Therefore, based on the capabilities and limitations fo

various techniques listed above, AES, XPS and SEM were used as the primary techniques. In this study, VG 310F Microlab AES and XPS, and Joel 840 SEM were used. For XPS, a Mg X-ray source was used and Field Emission Electron source was used for AES. The composition of the surface layer on the solder bumps at the die level was examined using AES and XPS, whereas SEM was used to measure the thickness and the morphology of the surface layer.

XPS and AES were performed on Pb/Sn solder bumps before and after BLM etch. From the Auger Analysis data, the percentage of each element in the layer was calculated to determine the dominant compound in the layer. For XPS analysis, since the spot size of XPS was larger than the bump size, a blanket wafer plated with Pb/Sn was used. The blanket wafer was agitated in an etch bath at elevated temperature for 10 minutes. The wafer was cleaved to scan across the layer using XPS.

3.2. Gravimetric Test of Pb Compounds

Solubility testing was used to verify the results. Solubility of different compounds was studied by dissolving them in the cleaning acid. First, each beaker was filled with 120ml of diluted 10% acid and the initial pH of the solution was measured using a pH meter. Then samples of 100% PbO, 97.4% PbO₂, 96.6% Pb₃O₄, 100% PbSO₄ and 99.9% SnO (manufactured from Baker Analysis and Mallinckrodt) were weighed and were dissolved in separate beakers. Agitation was provided with a stirring bar, and the reaction temperature and the change in color of the solution were recorded. After the solution was agitated for approximately five minutes, the solution was filtered using a funnel. The precipitant on the filter paper was dried in an oven. Then the final mass left on the filter paper was weighed and the solubility was calculated using this data. The final pH of the solution that was filtered through the paper was measured and recorded. Also, diluted 10% acid was buffered to a different pH to study the solubility of

Pb compounds in the acid. Those pH and solubility results were compared to the data given in the published Pourbaix diagram.

3.3. BLM Layer Etch Rate Study

To measure the etch rate of BLM layer in a lateral direction, a high sulfuric concentration of BLM etch bath was prepared at an elevated temperature in the 8 gallon bath. The dice were agitated in the bath for times ranging from 30 seconds to 5 minutes. A precision cross section of the corner of each die with different time intervals was performed through the middle of the bump to view the overetch of the BLM layer using SEM. This measured the undercut of the BLM layer underneath the bumps.

To obtain the etch rate in the vertical direction, blanket BLM layer deposited wafers were used. The wafers were premeasured on a RS55/tc Omnimap which is a device to measure the thickness of the wafer, to obtain initial thickness. The thickness of the blanket wafers were approximately 8000Å. Then each wafer was agitated in the same bath as above for times ranging from 5 seconds to 2 minutes. The final thickness was measured using the Omnimap. The difference between initial and final thicknesses was calculated. A graph was constructed to show the difference between the initial and the final thickness as a function of time.

CHAPTER 4. RESULTS AND DISCUSSION

4.1. Thickness Morphology and Composition of the Surface Layer of Solder Bumps

Precision SEM cross-sections were performed extensively to identify the thickness and morphology of the surface layer on Pb/Sn solder bumps. It was found that the morphology of the layer is critically dependent on the etchant concentration. H_2O_2 -rich solutions caused a very thin and dense surface layer as shown in Figures 4.1 and 4.2. However, as the concentration of H_2O_2 relative to H_2SO_4 increased, the layer appeared to be more loosely packed and thicker as shown in Figures 4.3 and 4.4. The morphology was independent of the etch time although the thickness increased with time.

Auger Analysis was performed on the bumps that were dipped in the H_2O_2 -rich solution of the BLM etch bath at an elevated temperature for 3 min and were reflowed in the furnace after they were cleaned with acid. SEM pictures of bumps are shown sequentially before dipping in the etch bath, after dipping in the bath, and after acid cleaning and reflow (see Figures 4.5-4.10). The composition of the surface of Pb/Sn bumps was obtained from the Auger analysis and is shown in Table 4.1. From this table, several observations can be made: Upon the exposure to the BLM etchant, S, Sn, Pb and O were found. The percentage of Pb increased after acid cleaning. This indicates that as the surface of the bump was cleaned with acid and reflowed, Pb was exposed. The level of Sn decreased after acid cleaning and reflow. During reflow, Sn formed an intermetallic layer with the BLM layer.

To find out about the bonding states of compounds, XPS was performed on the Pb/Sn plated blanket wafer with the same conditions as with the AES analysis. The limitation with XPS is that the difference in binding energy between Pb^{2+} and Pb^{4+} is less than 1eV. In addition, the charging effect causes peak shifts which make it harder to distinguish which peak the surface layer corresponds to (Tables for binding energy of

Table 4.1. Percentage composition of surface analysis using AES

Element/ % Composition	Before BLM etch (%)	After BLM etch (%)	After acid cleaning and reflow (%)
Pb	38.50	40.20	54.50
Sn	15.80	3.01	8.47
S	15.20	17.20	17.60
O	17.00	27.60	19.39
C	13.40	12.00	0.04

Pb compounds are listed in Appendix I). Samples of pure PbO, PbO₂ and Pb₃O₄ were used to standardize and calibrate the peak of each compound for accuracy. These XPS results are shown in Appendix II. The binding energy peak on the surface layer produced with the 86% H₂SO₄ etchant bath was close to the binding energy peak for PbO₂. Moreover, the atomic concentrations (%) of each element, before and after agitating in an etchant bath, are shown in Table 4.2. These quantitative XPS results were obtained using Wagner Empirical Sensitivity Factors [Handbook of X ray photoelectron spectroscopy] and the curve-fitting area under the XPS data. From these results, the concentration of S on the surface of the bumps after dipping in the BLM etch bath seemed high. Also, the percentage of S on the surface of the bumps increased by 10% after high sulfuric concentration bath exposure compared to the percentage of S after low sulfuric concentration. The percentage of S could be the reason for the difference in morphology of the surface layer. Based on free energy of formation tables shown in Appendix III, PbSO₄ is more stable than any other Pb oxide compounds.

Figure 4.1. The surface of Pb/Sn solder bumps after high sulfuric concentration bath (top view).

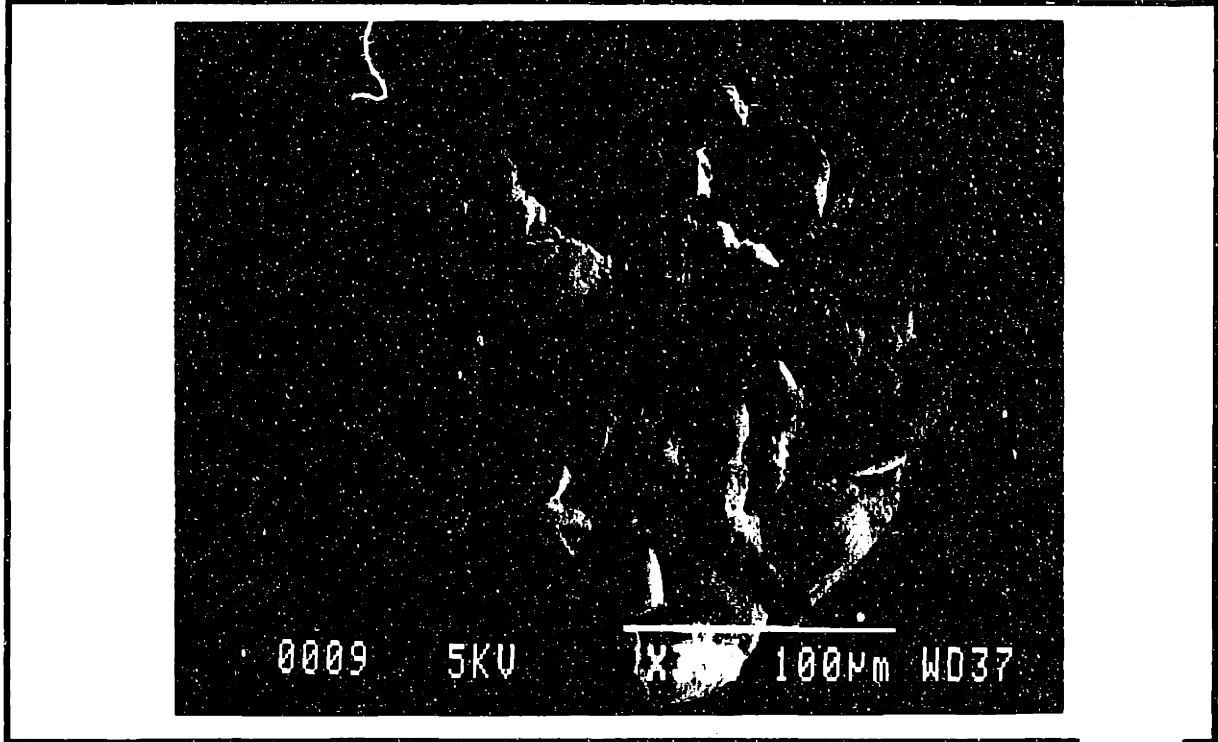


Figure 4.2. The surface of Pb/Sn solder bumps after same condition as Figure 4.1.



Figure 4.3. The surface of Pb/Sn solder bumps after low sulfuric concentration bath.

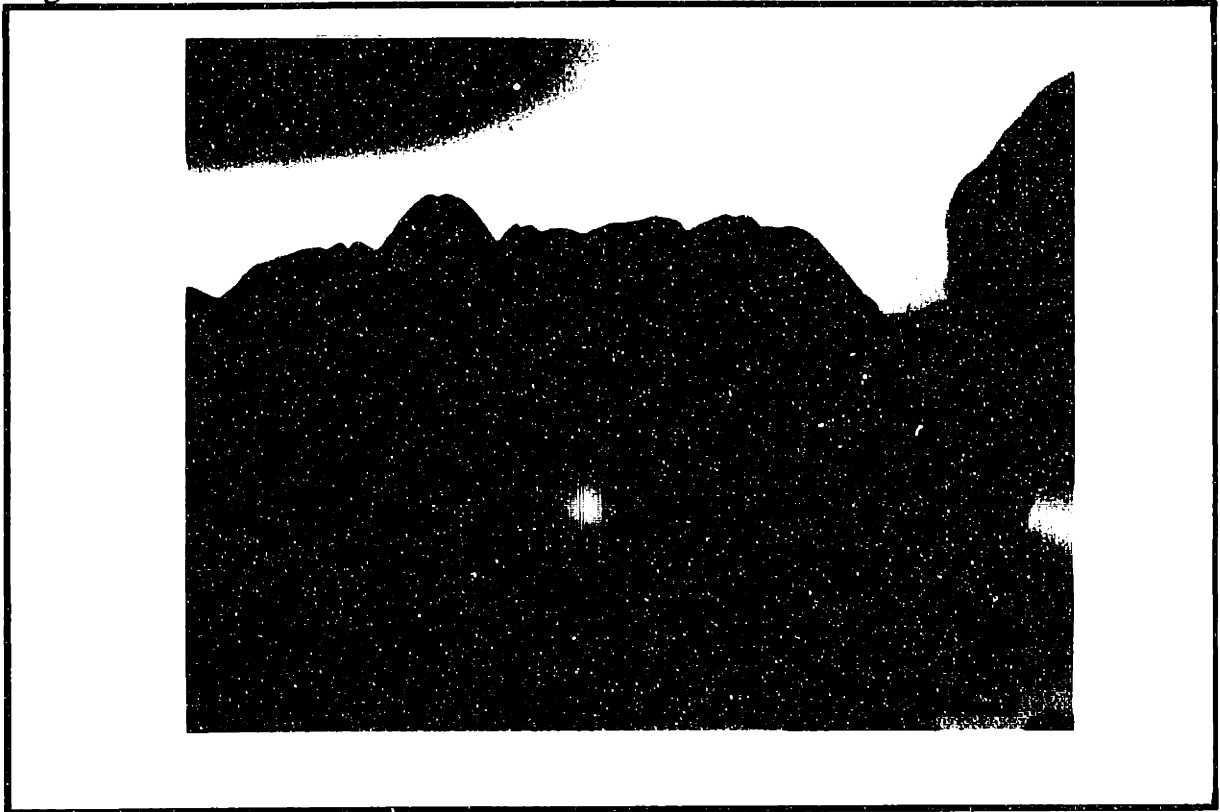


Figure 4.4. 2000X magnification

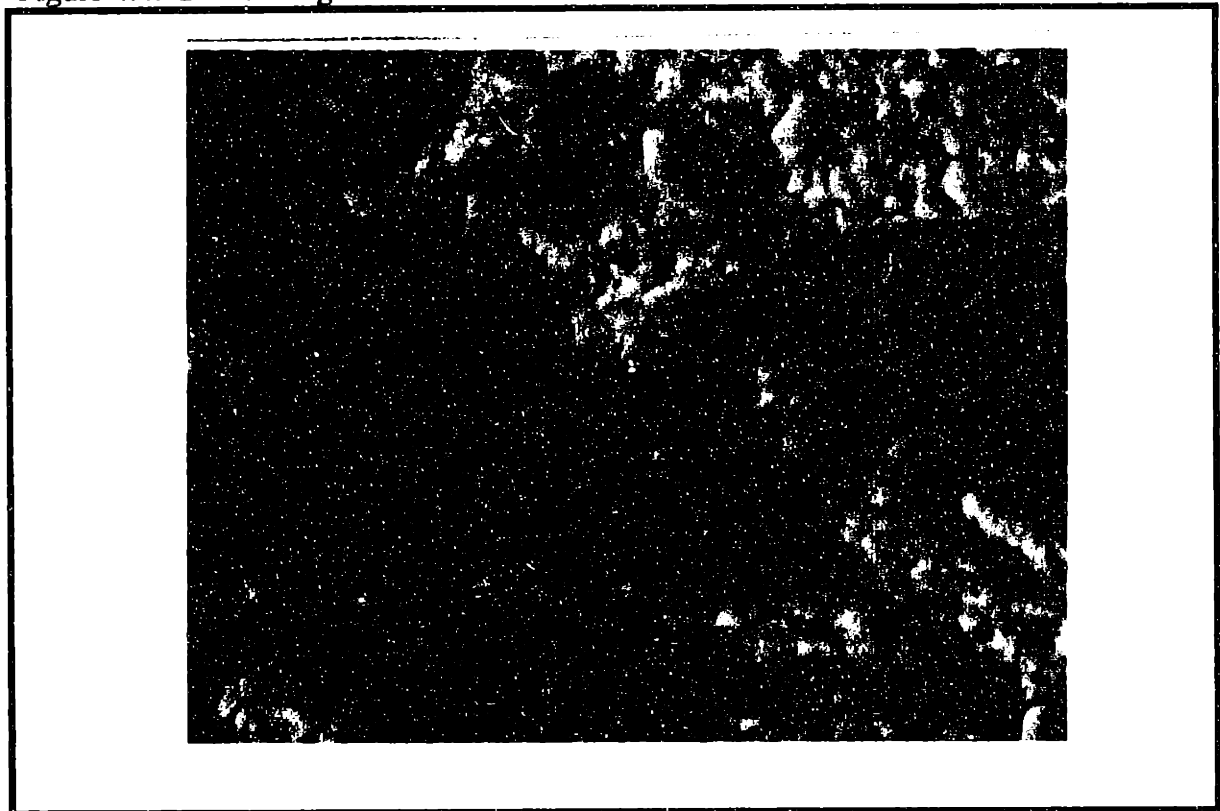


Figure 4.5. Solder Bumps before BLM etch

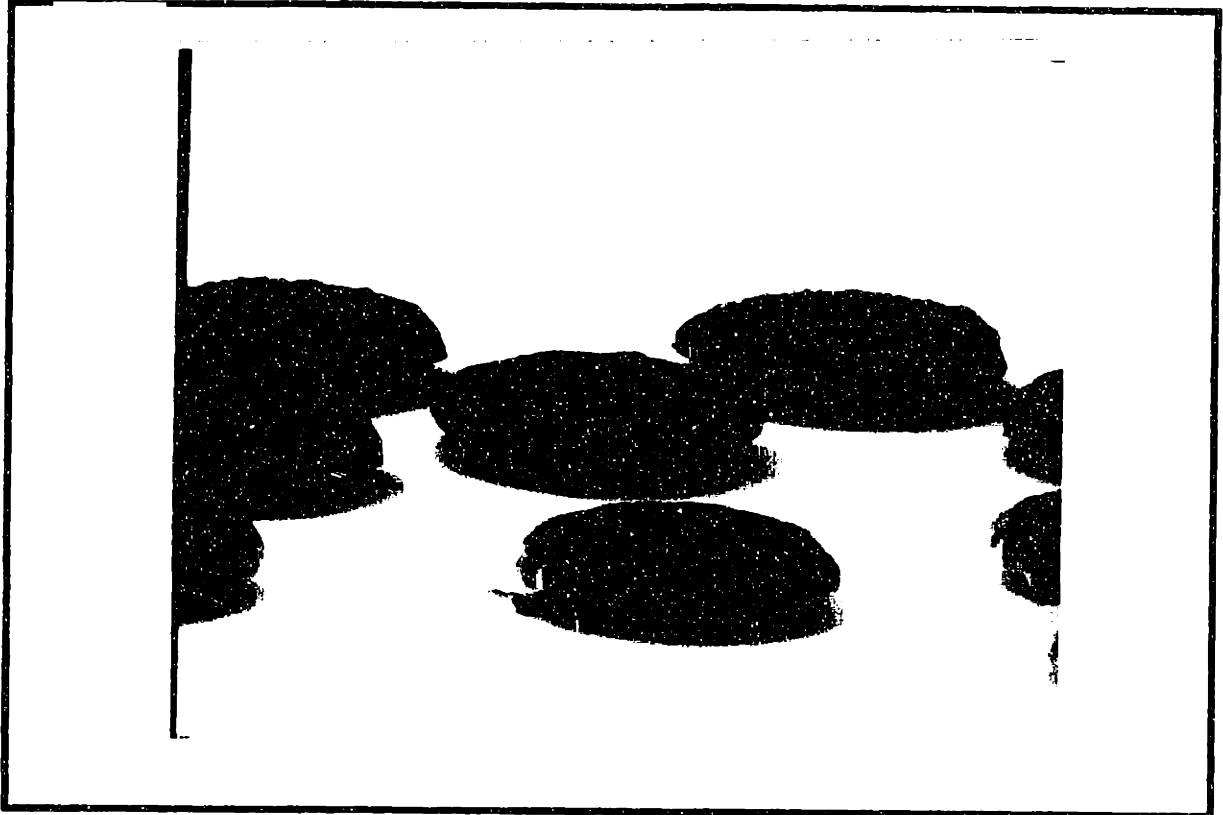


Figure 4.6. Solder bumps before BLM etch

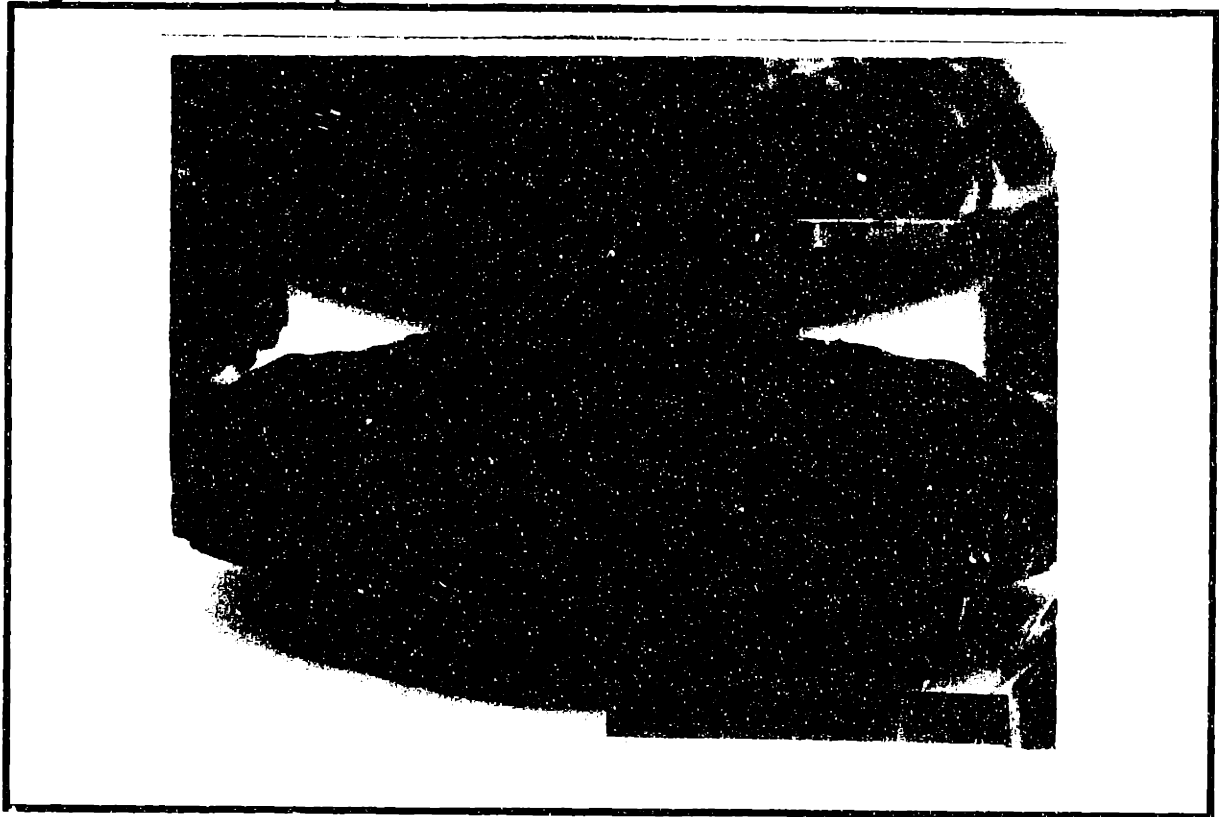


Figure 4.7. Solder bumps after BLM etch



Figure 4.8. Solder bumps after BLM etch

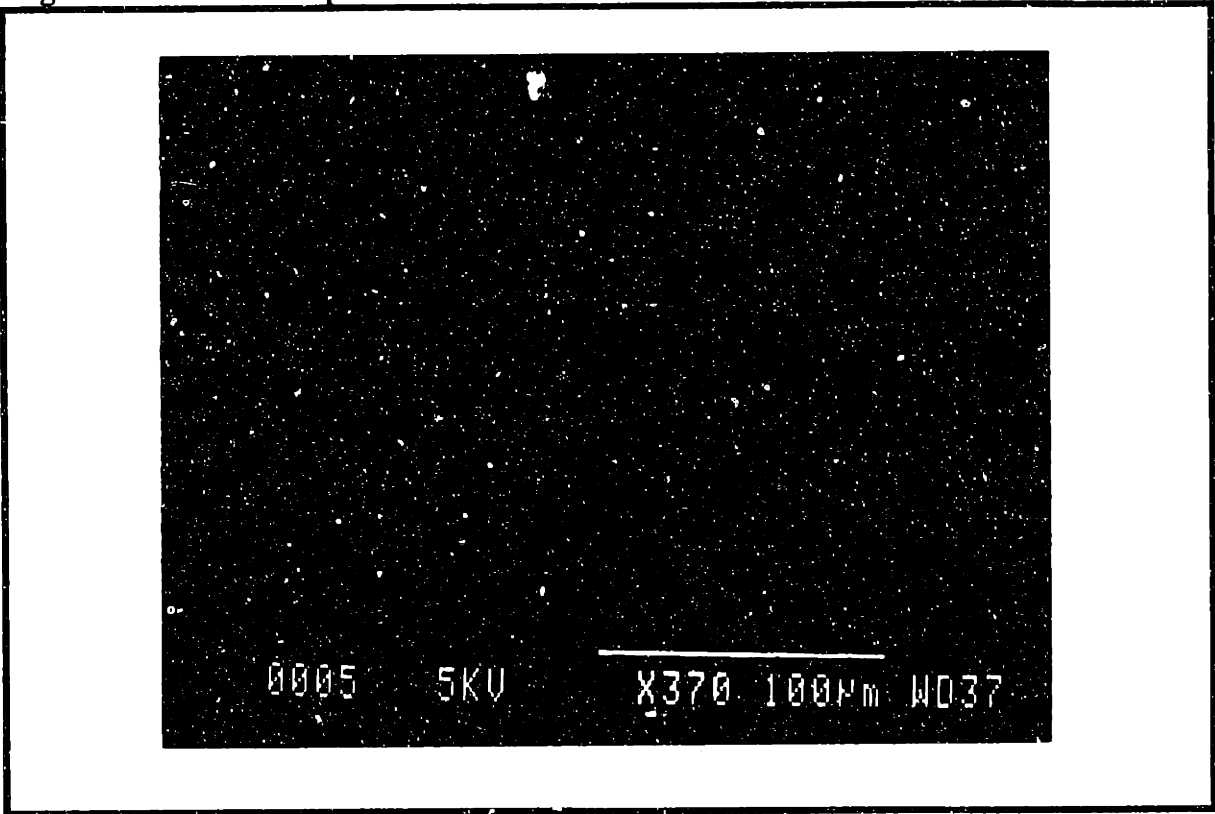
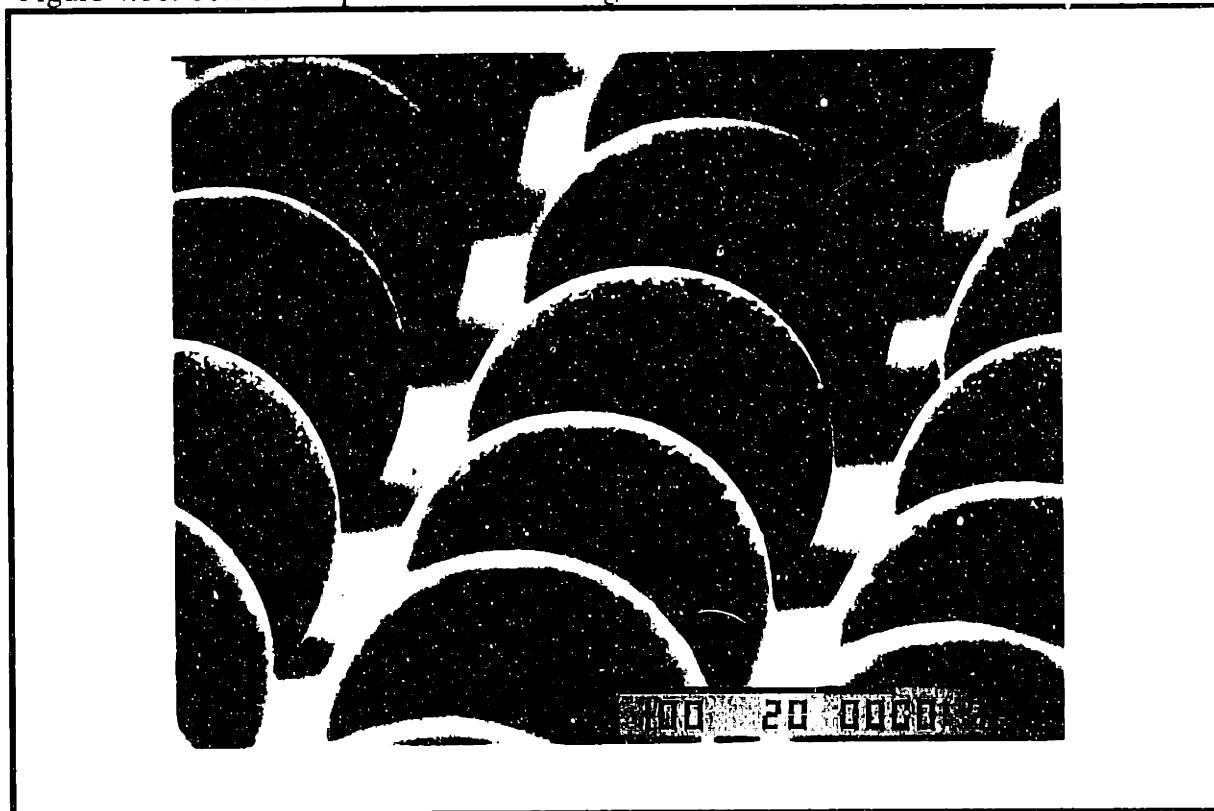


Figure 4.9. Solder bumps after acid cleaning and after reflow



Figure 4.10. Solder bumps after acid cleaning and after reflow



The concentration of sulfur was found to be higher at the top of the surface layer (Figure 4.11). Therefore, this scan showed that if the sulfur-compound is present in the

Table 4.2.

sample / % Composition	Pb	C	S	O	Sn
Pb/Sn bumps before BLM etch bath	28.1	20.6	0	47.9	3.4
Pb/Sn bumps after BLM etch bath	19.4	2.3	28.9	49.2	0.2

surface layer, it is most likely to be on the top of the layer.

According to the XPS results, the binding energy peak for the sample was determined to be 135.5 eV and the energy peak for PbO₂ is 136.3 eV, for PbO is 142.4 eV and for Pb₃O₄ is 143.0 eV. Therefore, the peak that is the closest to the peak of the sample is PbO₂ although the peak value is not within the given range as determined from the National Institute of Standards and Technology (NIST) data. The charging effect is the major reason for peak shifts and inaccuracies of peak values. The charging

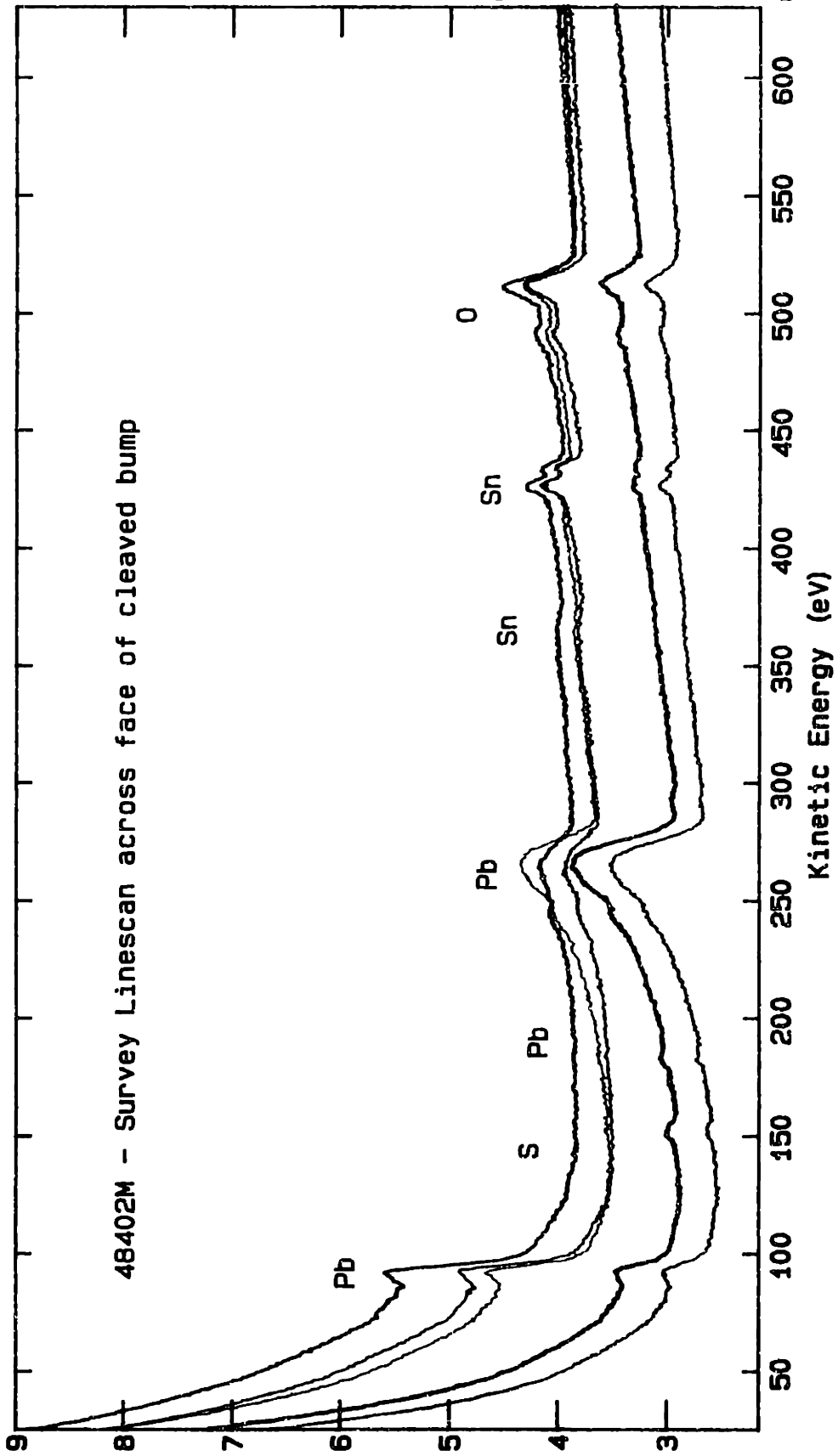
Table 4.3

Compounds	Binding Energy (eV)
Pb	136.4 -136.9
PbO	137.7-138.2
PbO ₂	136.8-137.6
PbSO ₃	138.6
PbSO ₄	139.4-139.5

effects and peak shifts are calibrated by the binding energy peak for C. The C peak is relatively high on these XPS results as shown in APPENDIX II. Moreover, the presence

of large quantities of C indicates that a lot of organic residues were left on the surface of Pb/Sn bumps. These residues might have originated from the Pb/Sn plating solution itself since the plating solution is based on a carbon compound. The XPS results indicate that the surface layer is most likely PbO₂, and the calculation of atomic concentration from percentages of 1Pb to 2O or 2Pb to 5O are shown in Table 4.2, also indicates that the layer is most likely PbO₂ or Pb₂O₅. However, the accuracy of this data is doubtful because of the charging effects and peak shifts in Bonding Energy peaks. Peak shifts occur due to charging and due to experimental environments. By looking at graphs of standardized peaks for Pb compounds, the C peak was found to be shifted more than 1 eV. So, the small binding energy peak difference between Pb²⁺ and Pb⁴⁺ makes it hard to distinguish between these peaks. Second, peaks between Pb compounds overlap to a certain extent according to the NIST data as shown in Table 3.4. A gravimetric test was then performed to verify these results.

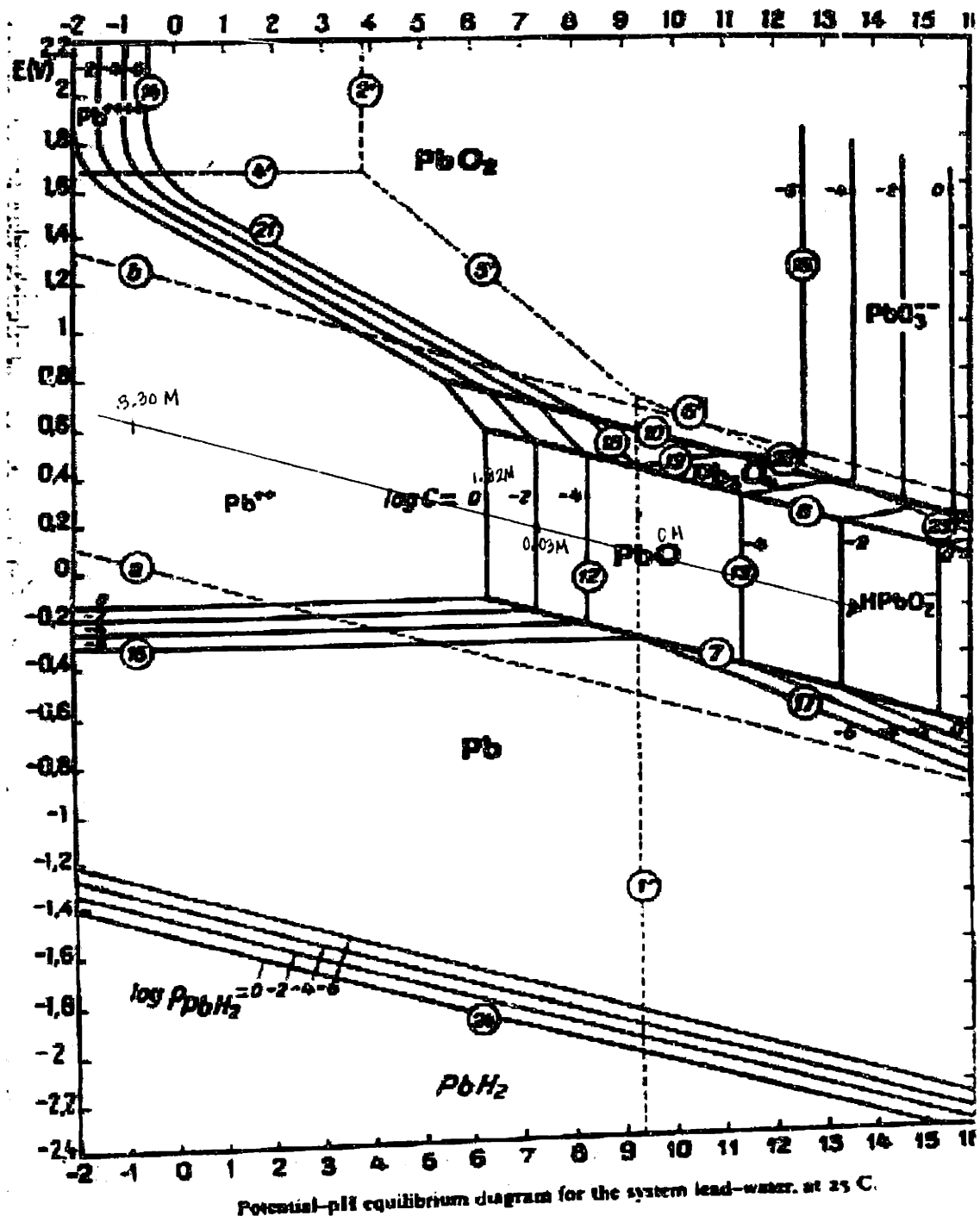
Figure 4.11. XPS scan on the cross section of Pb/Sn plated wafer after 86% H₂SO₄ bath.



4.2 Gravimetric Test

The Pourbaix diagram for Pb in the literature (figure 4.11) indicated that there are different regimes for Pb oxides, depending on the pH and the electrode potential of the solution. A gravimetric test was performed to identify the surface layer and also to confirm the XPS results. With a detection limit of 0.1 g/l, this gravimetric test was performed by dissolving several chemicals, such as PbO, PbO₂, PbSO₄, Pb₃O₄ and SnO, in the diluted 10% acid which removed the surface layer for reflow. The pH of the acid before dissolving any oxide was approximately -0.53. As a result, no chemical except PbO seemed to be soluble in the acid. Table 4.4 indicates pH before and after these Pb compounds were dissolved in the acid. From this table, PbO showed dramatic pH change whereas the other compounds showed slight pH changes. This indicates that only PbO reacted with the acid, whereas the other Pb compounds did not. These observations were also consistent with visual inspection. Pb compounds, except PbO, just remained in the bottom of the beaker giving a clear liquid on the top and the reaction temperature did not change. However, PbO showed very high solubility. When orange powder-PbO was put in 120ml diluted acid, bubbles were formed initially and the colors turned to light yellow. Moreover, the temperature increased to 45°C, indicating an exothermic reaction. When the solution was filtered, the solubility was approximately 405.6 g/l which is 1.82M. After the solution saturated, the pH was about 6.03 whereas the initial pH of the solution without PbO was -0.53. The pH and concentration for PbO in the acid matches with those in a Pourbaix Diagram for Pb compounds (Figure 4.12). In the PbO region, 1 M solution of PbO is in the aqueous state with pH close to 6.5. This figure closely matches with the experimental values which are 1.82M of PbO with a final pH of 6.03. Moreover, the graph indicates a decrease in concentration of dissolved PbO as the final pH becomes greater than 6.5. To demonstrate whether this is consistent with the experimental values or not, the acid solution was buffered to an initial pH of 13.0.

Figure 4.12. The trend of solubility of PbO in the Pourbaix Diagram for Pb Compounds



[source: Atlas of Electrochemical Equilibria in Aqueous Solutions, 1974, pp. 489]

Table 4.4.

compounds / pH	Initial pH (pH of 10% acid)	Final pH(after Pb compounds were dissolved)
PbO	-0.53	6.03
PbO ₂	-0.53	-0.39
PbSO ₄	-0.53	-0.28
Pb ₃ O ₄	-0.54	-0.28
SnO	-0.53	-0.56

The Solution showed very small solubility of PbO in the acid with pH of 13.0 that it was very hard to weigh the difference using filter paper. At final pH of 6.67 at saturated solution, the solubility of PbO showed about 0.032M. This result is consistent with the Pourbaix diagram in that the order of magnitude change in concentration of PbO resulted as the pH increased. As the final pH is less than 6.50, there is an increase in solubility. The 50% concentrated acid was prepared to observe the solubility of PbO in the acid with initial pH of less than -0.53. This reaction gave off heat, increasing the temperature to 75 °C. PbO consumed acid, resulting in white blocks of crystals. The solubility seemed to be high but the solution was very dense during filtering through the funnel. The solubility of PbO in the acid with an initial pH of -1.02 was about 747.5 g/l or 3.35M at the saturated level. The trend of solubility is shown with an arrow in the Pourbaix diagram (Figure 4.12): The solubility of PbO is the highest at a pH of -1 and the solubility decreases gradually at other pHs. Therefore, the bulk gravimetric test indicates that the surface layer of Pb/Sn solder bumps is composed of PbO, having a solubility of 3.35M at a final pH of -1.02 at saturated level and the solubility of PbO is favorable till the final

pH reaches 6.03 with a saturated concentration of 1.82M . Solubility of PbO with different pH is summarized in Table 4.5.

From the table 4.4, PbSO₄ was not soluble and this result matches with the XPS analysis result; therefore, this solubility test confirms the absence or a very small concentration of PbSO₄ in the surface layer. The identification of the surface layer contrasts with the results from XPS in that PbO is the probable surface layer instead of PbO₂. Because of several limitations and inaccuracies that XPS has in view of the

Table 4.5.

Initial pH	Final pH	Conc. (M)	Observation
-1.02	-1.02	3.35M	50% concentrated acid, white dense crystals formed and the temp. was 75 °C.
-0.53	6.03	1.82M	Solution turned to ivory yellowish color and the temp. increased to 47 °C (10% acid).
0.77	6.66	0.032M	Solution turned to white color with reaction temperature of 55 °C (10% acid).
1.06	9.87	0	PbO did not dissolve in the acid, maintaining its orange color at room temperature (10% acid).
13.10	13.24	0	same as above except that the color of PbO was heavy orange (10% acid).

apparent solubility of PbO in acid, a bulk solubility test appears to be more accurate than the spectroscopic analysis. Therefore, S, Sn containing PbO, is believed to be the layer that has formed on solder bumps by reacting with H₂SO₄ and H₂O₂.

4.3. Reaction Mechanism for Surface layer growth studies of Solder Bumps

To study surface layer growth with the concentration effects of H_2O_2 and H_2SO_4 , concentration of H_2O_2 was varied with a constant ratio of H_2O and H_2SO_4 . The etch time was four minutes for each set of experiments. The thickness of the surface layer was measured by taking a cross section of the die (The result is shown in Figure 4.15). As shown in figure 4.13, as the concentration of H_2O_2 increased, the surface layer thickness increased dramatically, proportional to the concentration level of H_2O_2 . In the low concentration of H_2O_2 , up to 35% of H_2O_2 solution bath, the surface layer growth rate did not increase as fast as it did in the 35% or higher concentrations of H_2O_2 . In the regions of 0 to 35% H_2O_2 solution, 65-100 % H_2SO_4 concentration is present. In that region, the thickness of the surface oxide layer was thin (less than 5 μm). In the region of more than 35% H_2O_2 , the growth of the layer grew at a faster rate, resulting in a very loose layer of up to 45 μm as shown in Figure 4.15. These regions are not favorable although BLM gets etched fast. It is difficult to remove those thick oxide layers and a dramatic volume loss in bumps resulted. The rapid growth of the layers consumes the bump height by oxidation, and a faster growth rate of the surface layer will eventually result in uneven bump height which is not favorable from a processing point of view. Since this region forms loose layers where there is no sulfate layer on the top to prevent the layer from growing fast, the reaction rate is a lot slower than the diffusion rate. Therefore, the reaction rate is controlling the growth rate. At 100% H_2O_2 , the surface layer thickness reached its peak at 50 μm . As shown in the SEM picture (Figure 4.16), the layers are not noticeable because the layers remain loose and slough off when no H_2SO_4 is present. Many layers got washed away during rinsing, resulting in a 50 μm bump height reduction. Moreover, pure H_2O_2 did not etch the BLM layers at all. Therefore, rich concentrations of H_2SO_4 prevent a fast growth rate of surface layer formation and promote a BLM etch. From figure 4.13, at 95% of H_2O_2 , the thickness of the layer dropped about 5 μm , resulting in a drop in the bump height.

Figure 4.13.

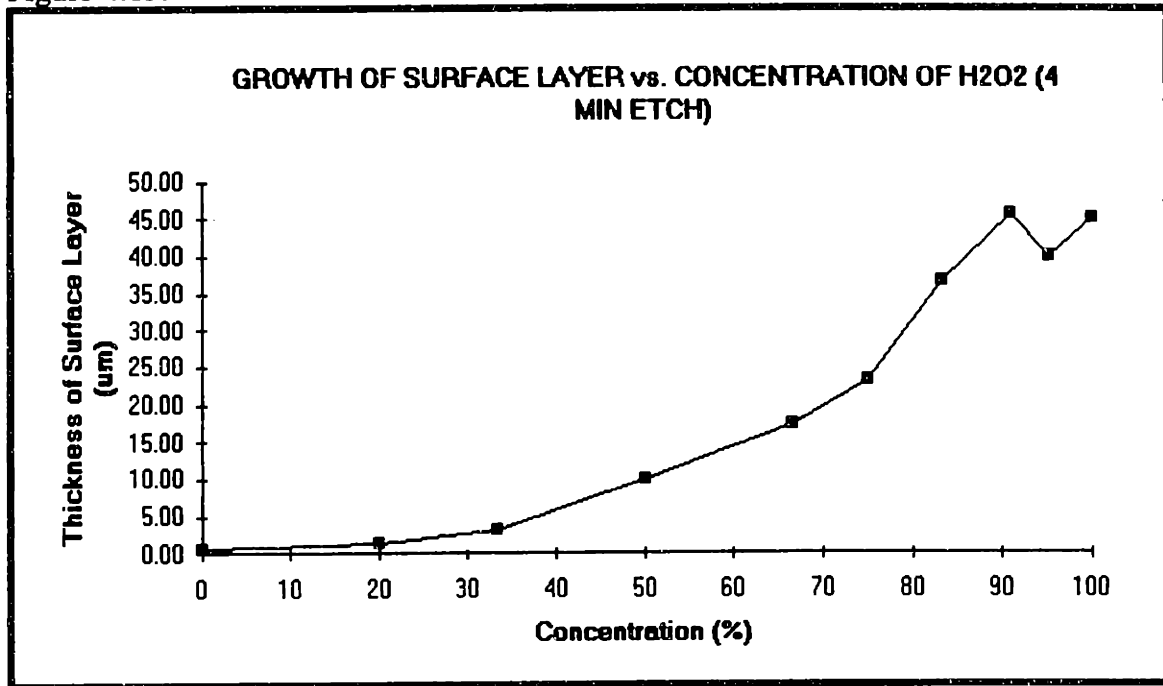
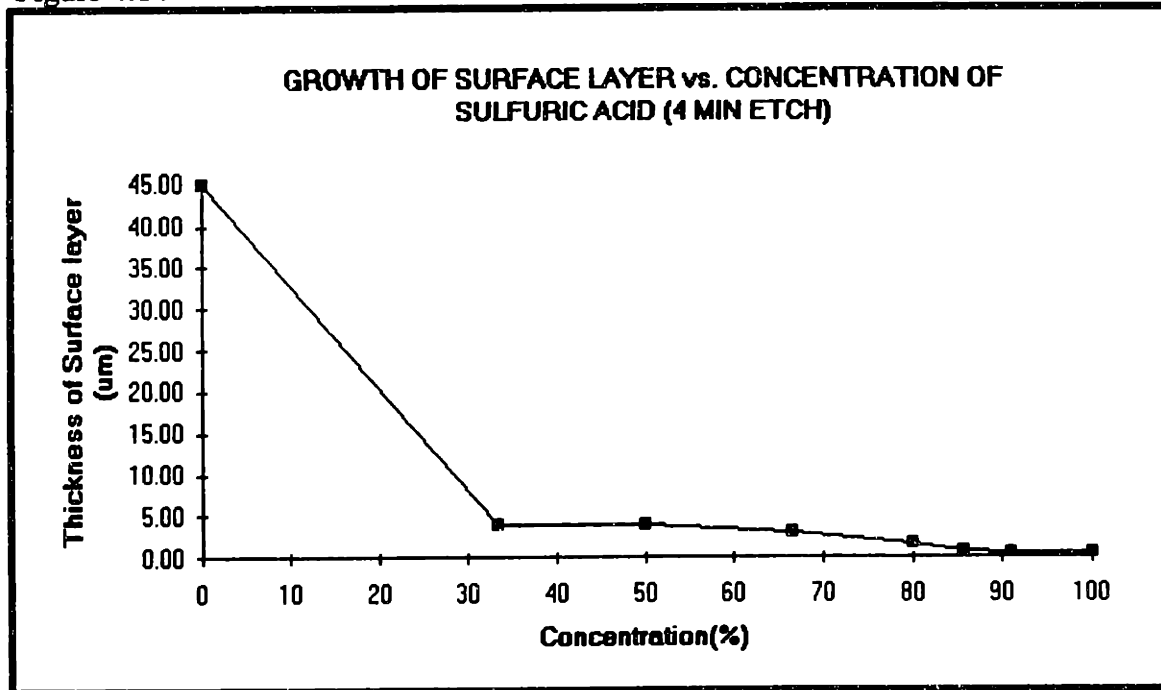


Figure 4.14



At that very high concentrated H_2O_2 solution, the resulting thickness is very flaky and uneven, and it is difficult to measure accurate thicknesses of layers. An accurate thickness of the layers would be about 5 μm higher. The right proportion of H_2SO_4 and H_2O_2 is necessary to etch a BLM layer completely around the bump and to form a thin surface layer at the same time.

The previous studies in this paper showed the effect of concentration variation in H_2O_2 by keeping the other ratios constant. The effect of concentration variation in H_2SO_4 by keeping the other ratios constant was studied to further investigate the impact of H_2SO_4 on surface layer growth. The exact conditions as described above was applied in these experiments. SEM pictures for cross sections at different concentrations are shown in Figures 4.17-4.24. Keeping these ratios constant, only the ratio of H_2SO_4 varied with respect to the other two components. As shown in that figure (4.14), concentrations of 0 -30 % H_2SO_4 showed a dramatic decreasing trend in the thickness of the surface layer, resulting in a final thickness of 5 μm at 30% H_2SO_4 from the initial thickness being 45 μm . At 0% H_2SO_4 , only oxidation of Pb/Sn solder bumps takes place. As the percentage of H_2SO_4 increased, the thickness of the surface layer decreased dramatically until the concentration of H_2SO_4 reached around 35%. Then, the thickness of the layer seems to stabilize at an average of about 5 μm . Therefore, H_2SO_4 plays a significant role in making layers denser or thinner. Up to 35% of H_2SO_4 concentration, the growth rate of the surface layer of the solder bumps are rapid through the diffusion of the BLM etchant. This rapid growth is limited by the reaction rate where the thickness growth is proportional to the time. However, more than 30% of the H_2SO_4 concentration results in very low thickness of the surface layer, showing no dramatic change in thickness of layers. In that region, because the diffusion rate is the rate-determining step, the growth of the layer is slow. The overall thickness of the surface layer after 35 % H_2SO_4 concentration was approximately 5 μm . The thickness difference between 30% and 100% H_2SO_4 was less than 3 μm as shown in Figure 4.26.

Figure 4.15. Cross section of Pb/Sn solder bumps after 90% H₂O₂ bath (4 min etch)

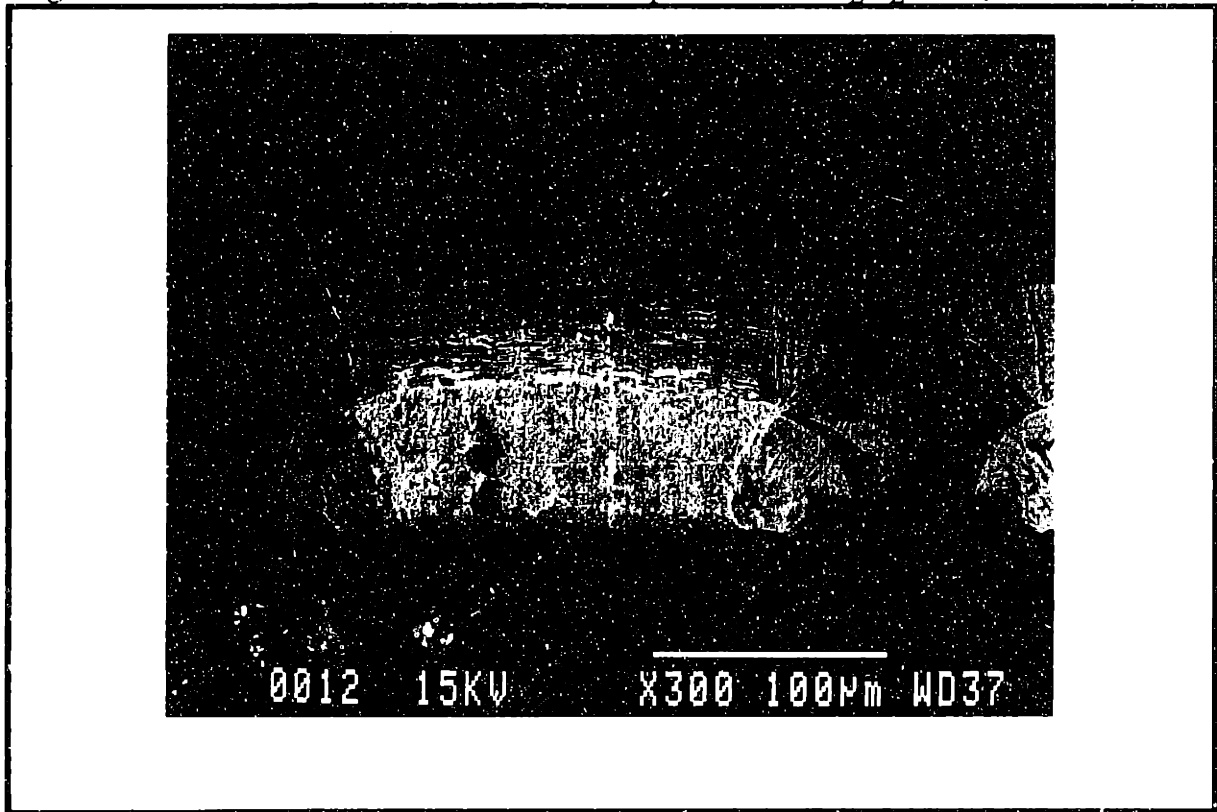


Figure 4.16. Cross section of Pb/Sn solder bumps after 100% H₂O₂ bath (4 min etch).

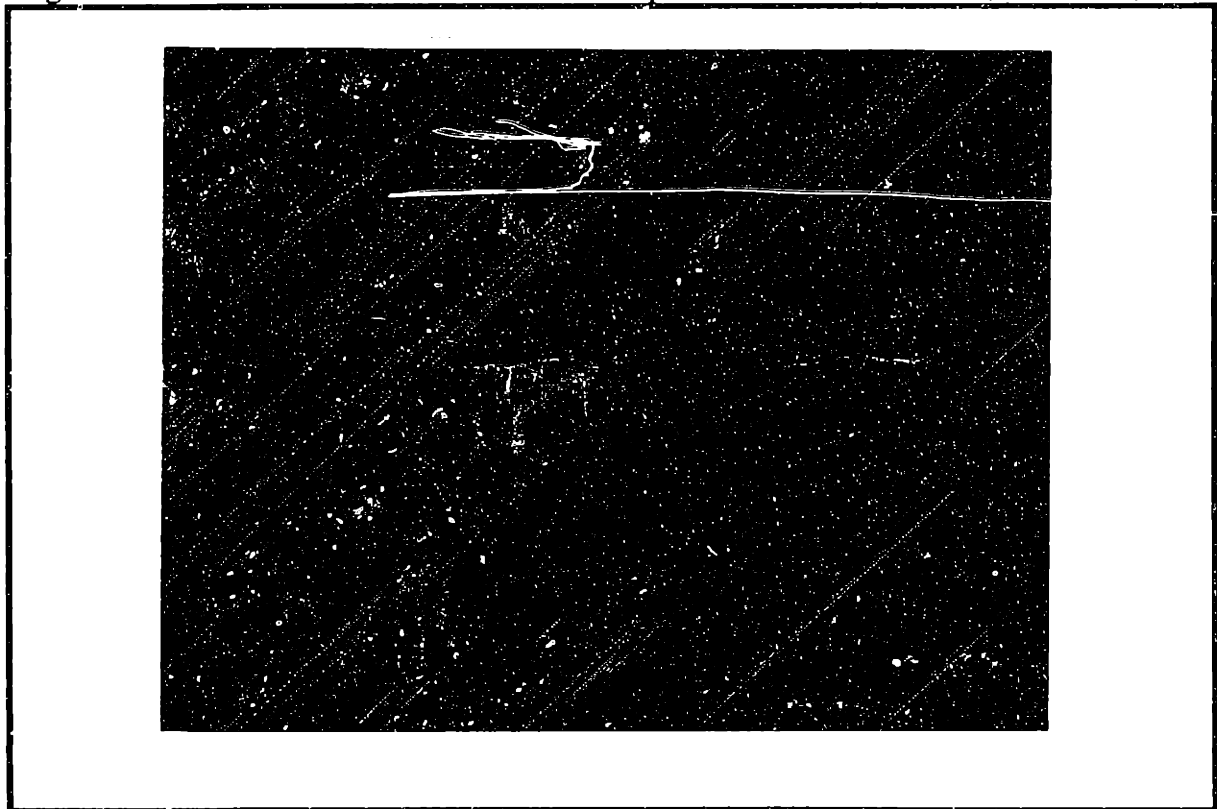


Figure 4.17. Cross section of Pb/Sn solder bumps after 100 % H₂SO₄ bath (4 min. etch)

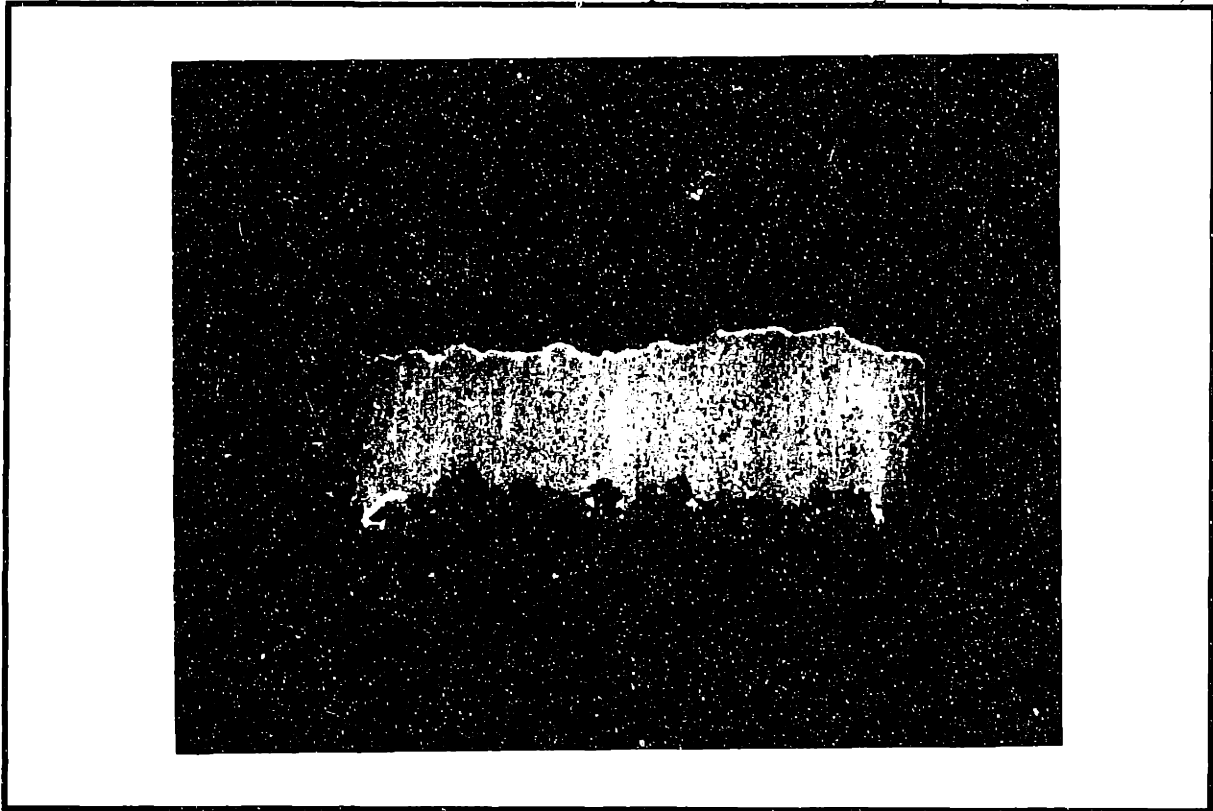


Figure 4.18. Cross section of Pb/Sn solder bumps after 33% H₂SO₄ bath (4 min. etch)

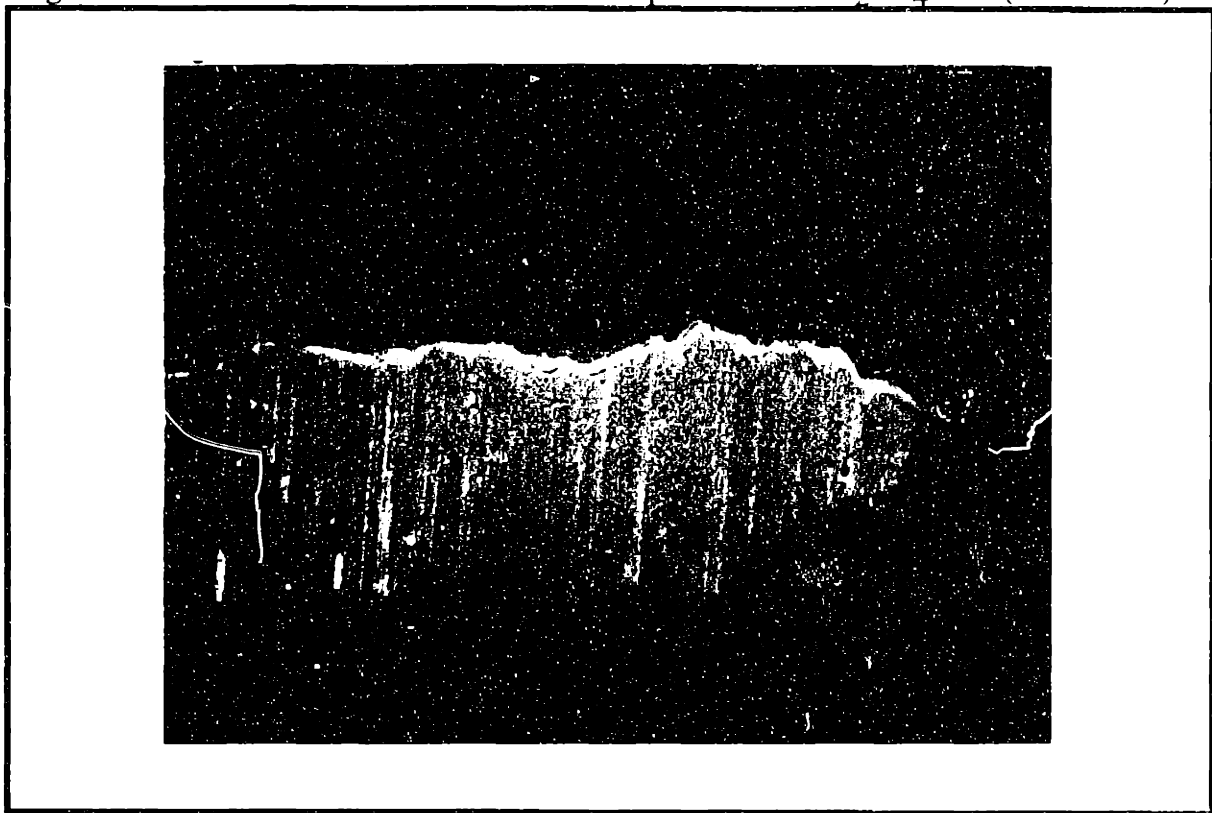


Figure 4.19. Cross section of Pb/Sn solder bumps after 50% H₂SO₄ bath (4 min. etch)

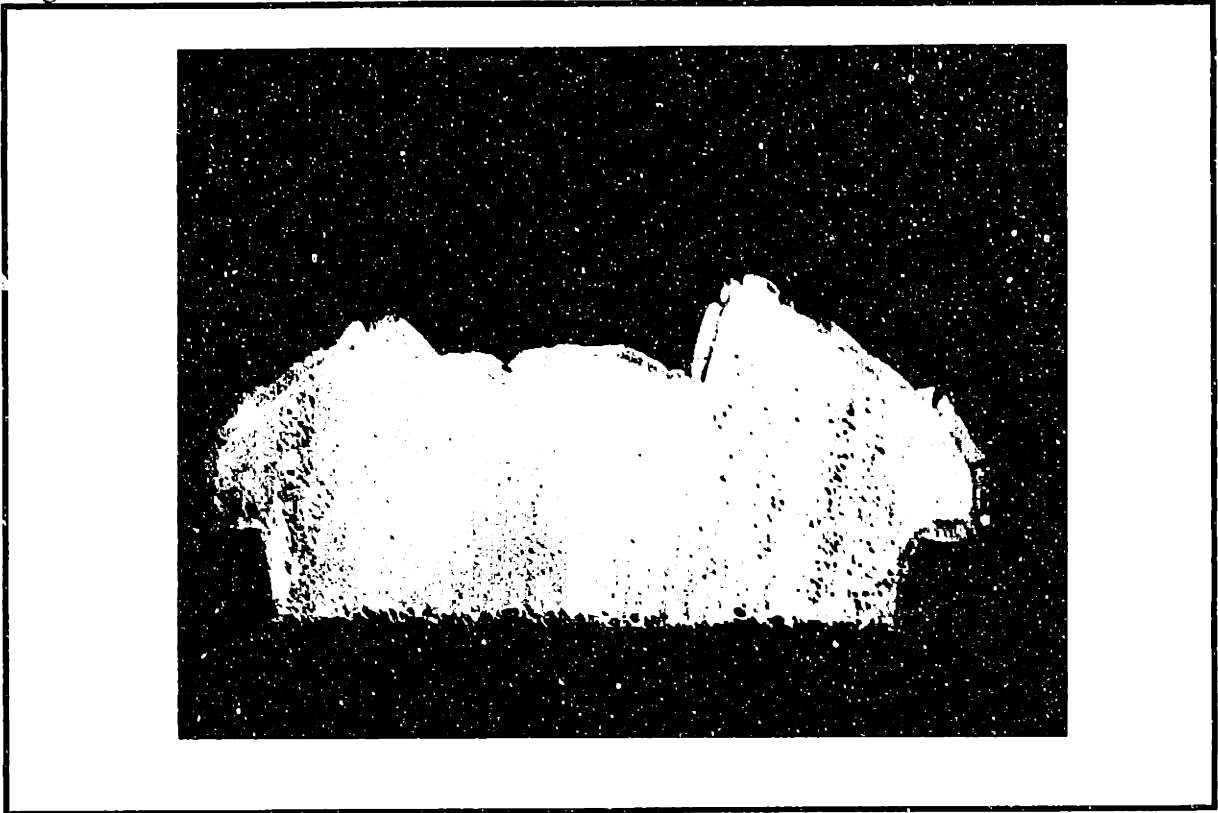


Figure 4.20. Cross section of Pb/Sn solder bumps after 66% H₂SO₄ bath (4 min. etch)

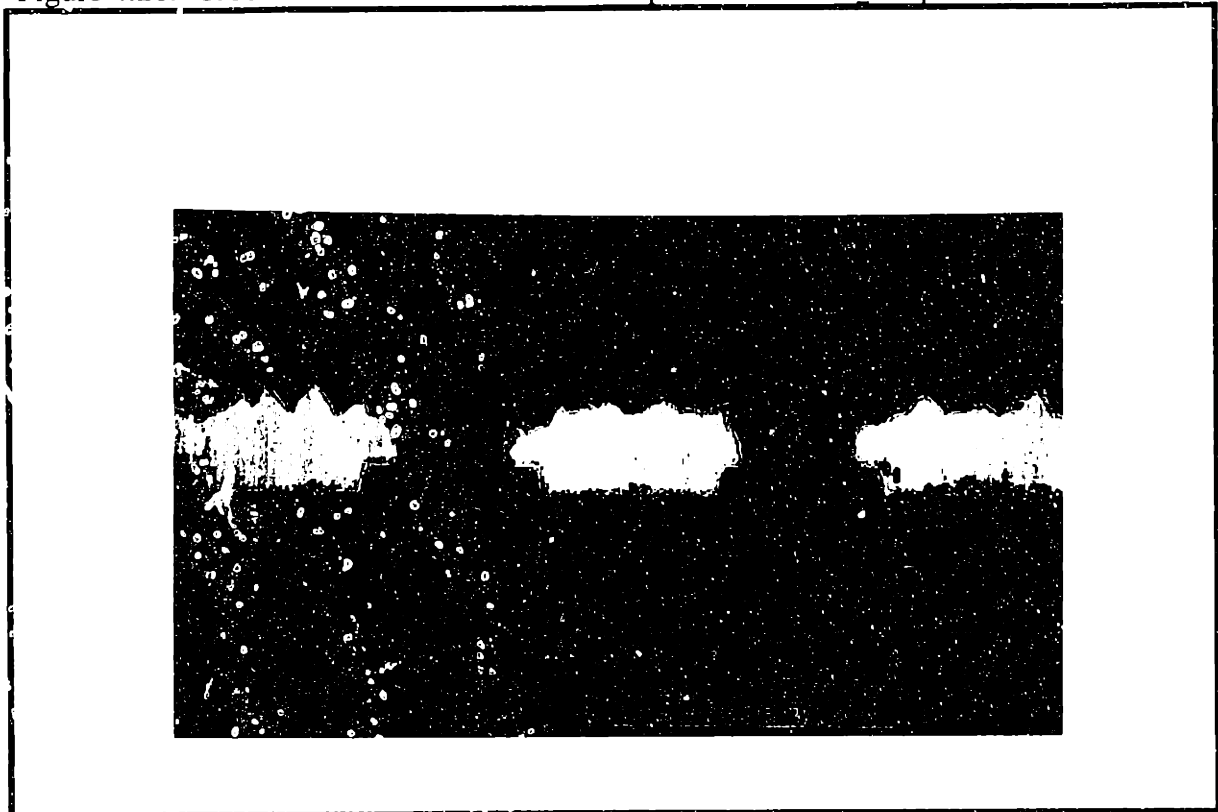


Figure 4.21. Cross section of Pb/Sn solder bumps after 80% H_2SO_4 bath (4 min. etch)

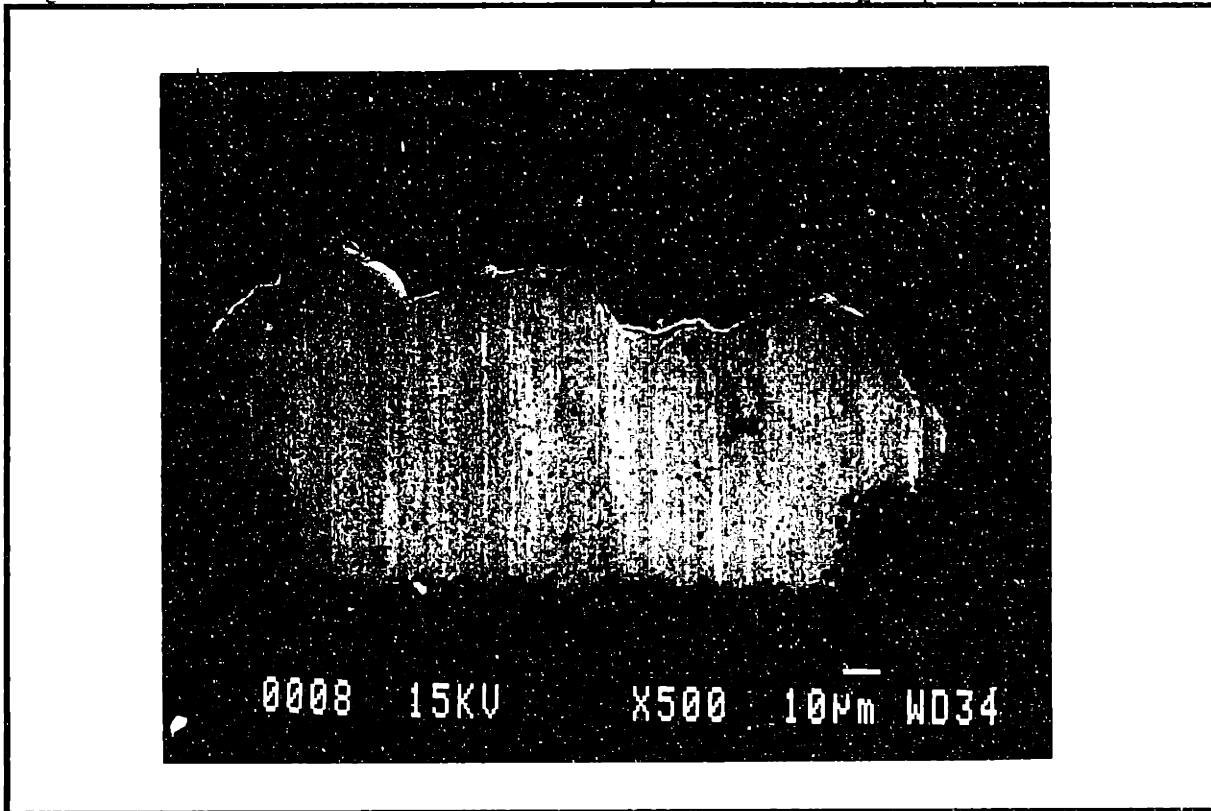


Figure 4.22. Cross section of Pb/Sn solder bumps after 86% H_2SO_4 bath (4 min. etch)



Figure 4.23. Cross section of Pb/Sn solder bumps after 91% H₂SO₄ bath (4 min. etch)

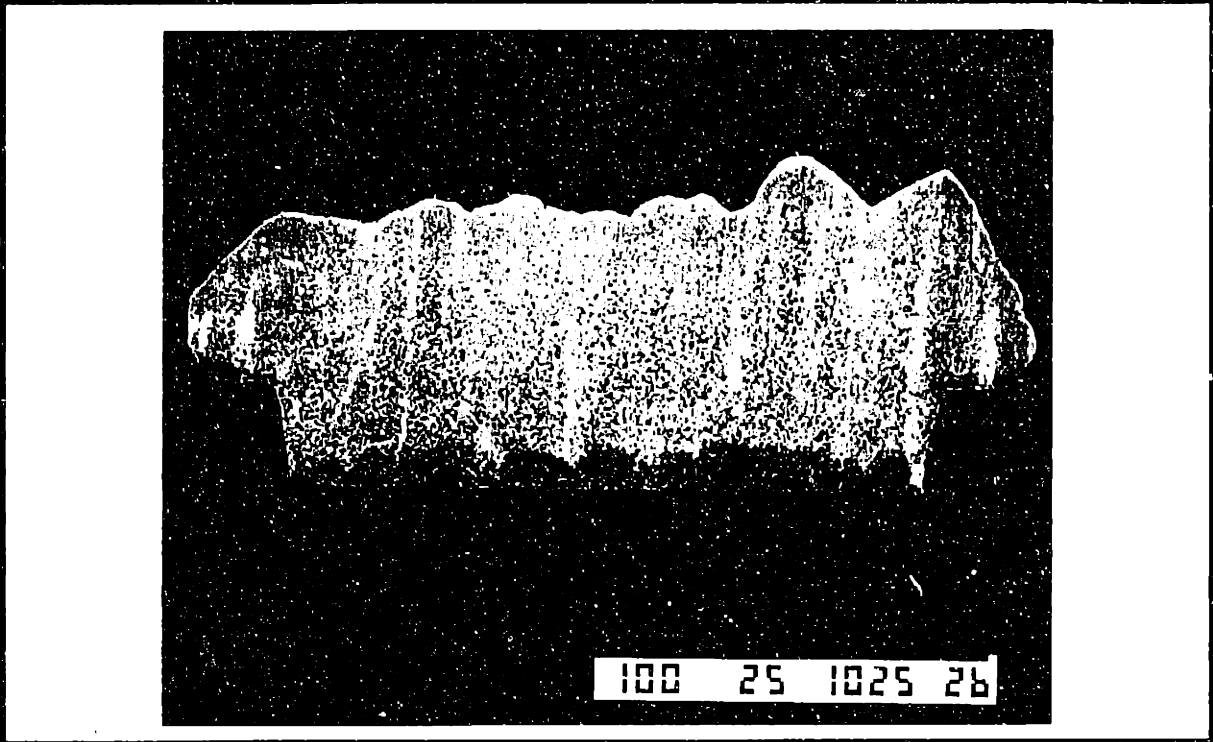


Figure 4.24. Cross section of Pb/Sn solder bumps after 100% H₂SO₄ bath (4 min. etch)

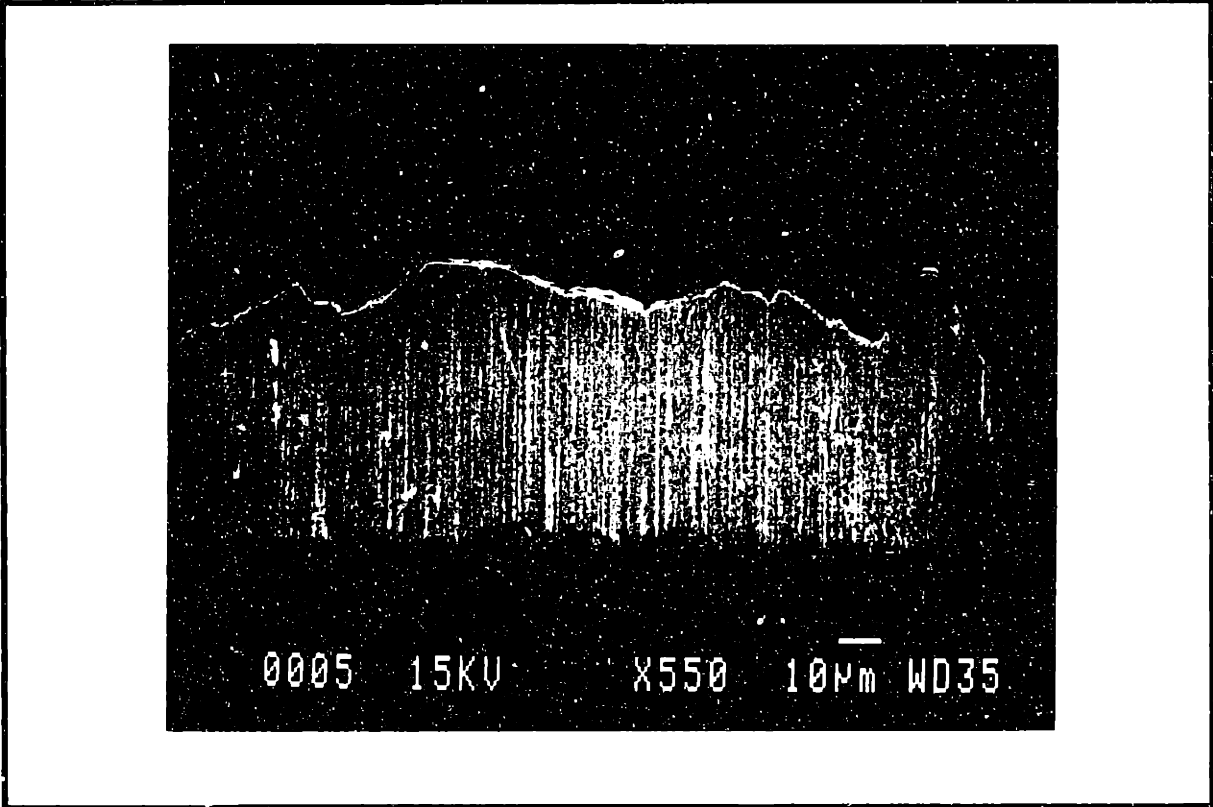


Figure 4.25

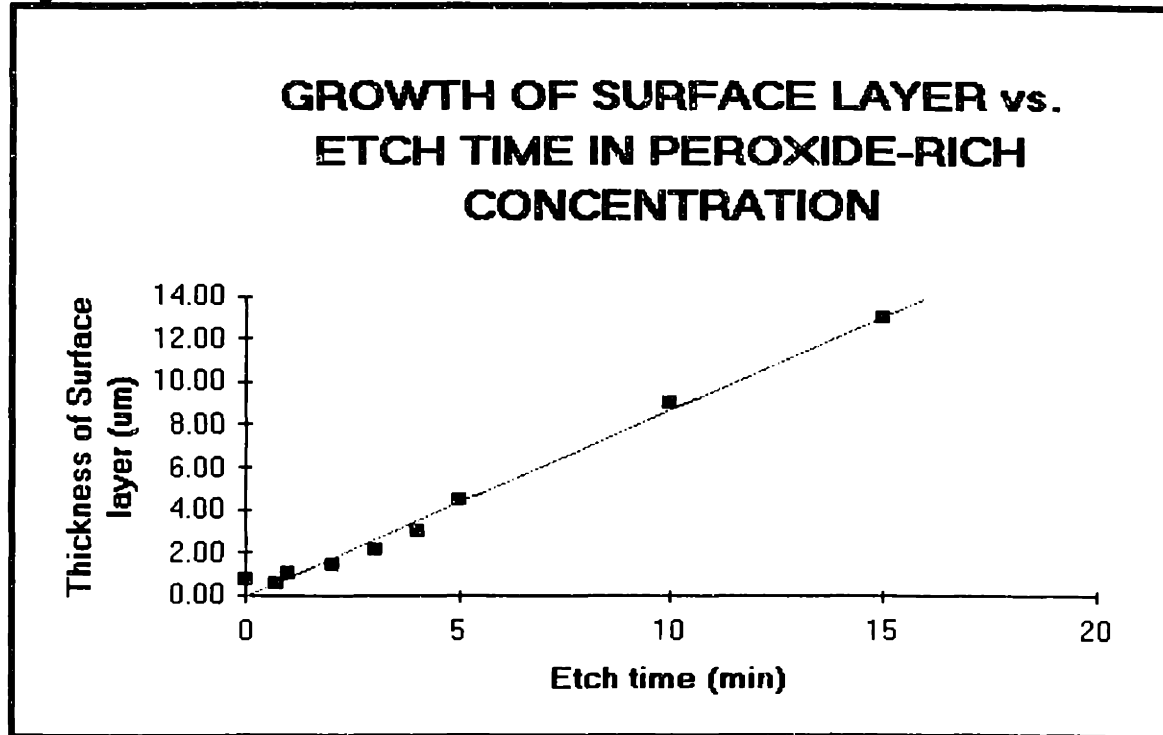
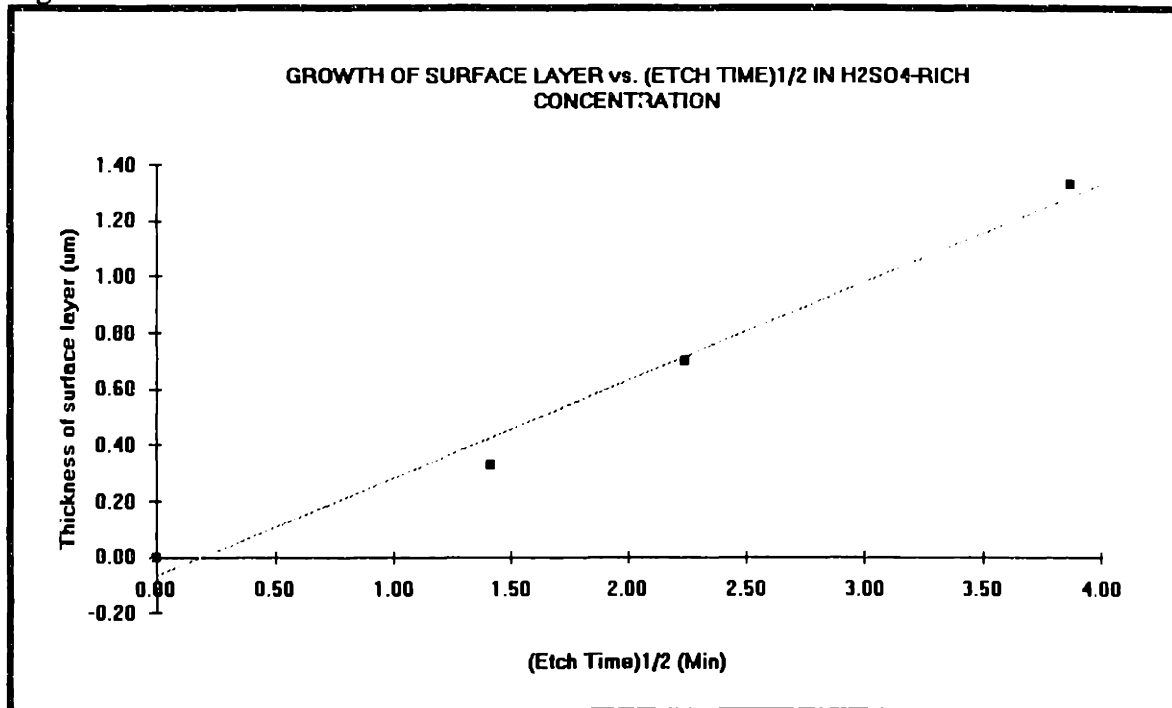


Figure 4.26.



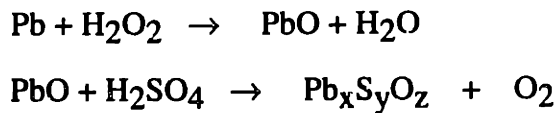
At 35% concentration of H₂SO₄, the layer decreased from 5 μm, eventually going down to 1 μm at 100% H₂SO₄. From these studies, having a large percentage of H₂SO₄ in solution will result in a zero order reaction where the thickness of the surface layer is less than 5 μm. Also, having a thin layer will make it easier for the acid to remove so that these Pb/Sn bumps can be reflowed.

A combination of H₂SO₄ and H₂O₂ with high concentration of H₂SO₄ is necessary, not only for the thin surface layer, but also for a fast BLM etch. Using these two figures, an optimal BLM etch solution concentration can be determined. 86% H₂SO₄ region is the optimal etch concentration, where the BLM is completely etched around bumps after 4 minutes and the surface layer is about 1 μm thick. At 86% sulfuric acid, the reaction of surface layer growth is limited by the diffusion rate, resulting in slow growth of the layer. Therefore, this concentration study suggests the optimal etch concentration.

In H₂O₂-rich solution, the surface layer of Pb/Sn bumps appeared to be loose and thick. Also, it was found that the surface layer grew linearly with time as shown in Figure 4.25. The growth rate of the surface layer was approximately 1.1 μm/min. Since the growth rate of the layer is linearly proportional to time, this etch reaction is reaction-rate limited instead of diffusion-rate limited. Since the layer is loose and flaky, the etchant is diffusing quickly through the layer, promoting the growth of the layer. The concentration studies from figures 4.13 and 4.14, demonstrate this result. The reaction rate is the rate-determining step.

In sulfuric acid rich solutions, the morphology of the surface layer seemed to be dense and thin. It was found that the surface layer grew linearly with the square root of time as shown in Figure 4.26. Since the layer is dense and thin, this surface layer is preventing the etchants from diffusing through the layer quickly; so the layer growth is slow. This surface growth is diffusion-rate limited. From the results obtained, S seems to be the reason for the differences in thickness morphology and reaction mechanism.

Moreover, the increase in percentage of S in the surface layer (Table 4.2) in the sulfuric-rich solution according to AES scan, suggests S being the source of these differences. Free energy tables (Appendix III) show PbSO₄ being stable over any other Pb oxide compounds, which also supports the impact of S on the surface layer. However, the gravimetric test showed that PbSO₄ is not soluble in the cleaning acid. Therefore, the surface layer is some type of sulfate compound where the most of the surface layer is made of lead oxide with a very small percentage of non-uniform sulfate layer on the top of the bumps. Although the sulfate layer is not primarily taking part in the stoichiometry of the compound, the thickness and the density of the surface layer is controlled by the very small concentration of sulfate layer on the top of the bumps. Based on these results, the following reaction for the surface layer growth on the Pb/Sn solder bumps was proposed:



4.4. BLM Layer Etch Rate Studies

So far, we have studied surface composition analysis of solder bumps in a BLM etch bath. To answer the question how fast are H₂SO₄ and H₂O₂ etching the BLM layer, etch rates of BLM layer in a lateral and vertical direction was determined. It was found from the concentration variation studies that the 86% H₂SO₄ etch bath creates a thin surface layer on Pb/Sn bumps and etches the BLM layer at a fast rate. During the time it takes to create a layer on Pb/Sn solder bumps, the BLM layer surrounding the bumps is etched off completely. To study the etch rate of the BLM layer in a lateral direction (Figure 4.27), a cross section of bumps, through the center of the bump, was studied using the SEM (Figure 4.28 and 4.29). The condition for the etch bath is 86% H₂SO₄ with varying time. Since this etch reaction is isotropic, the etch rate in a vertical

Figure 4.27. Diagram of BLM layer in a lateral and vertical direction

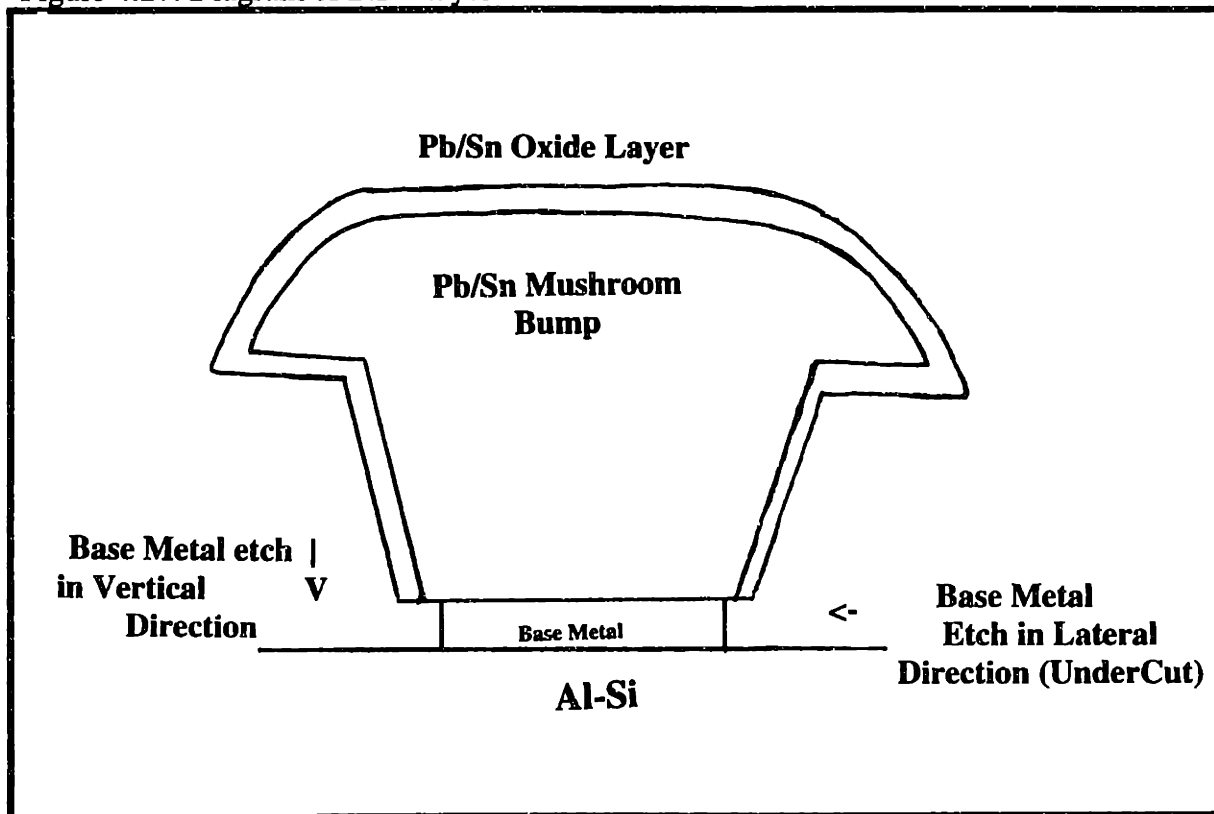


Figure 4.28. The undercut of BLM layer after 86% H₂SO₄ for 1 min.

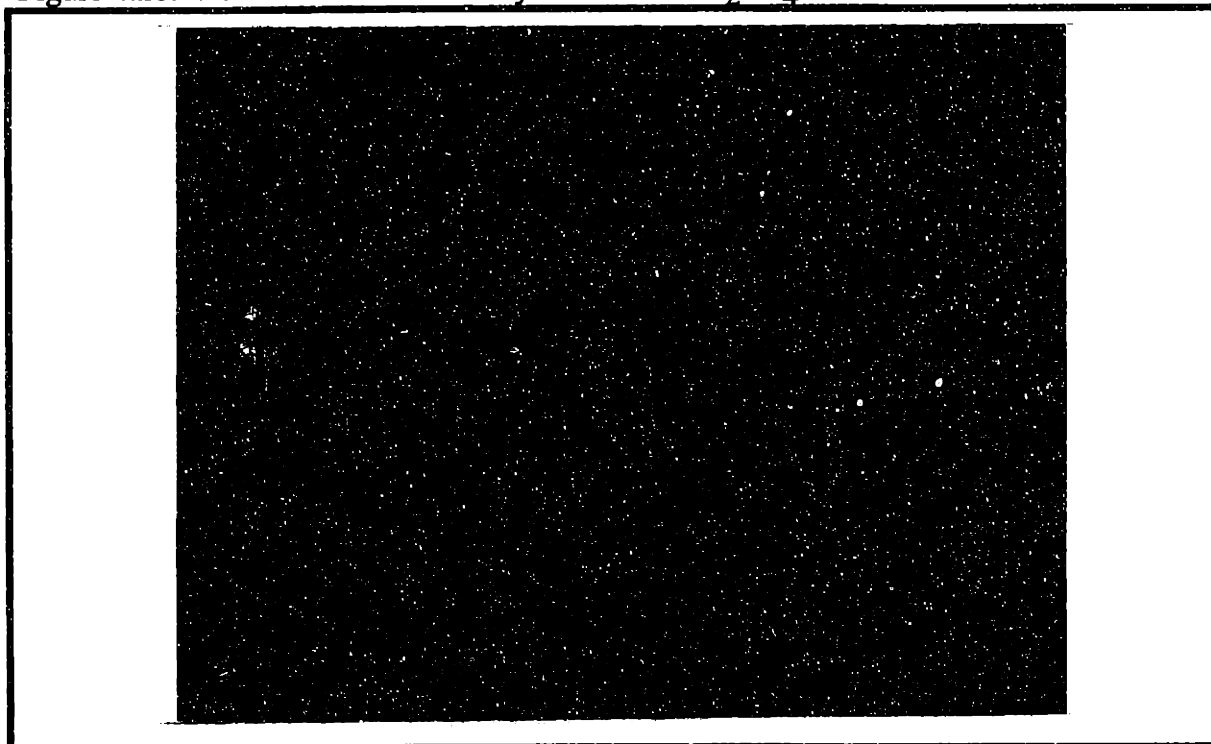
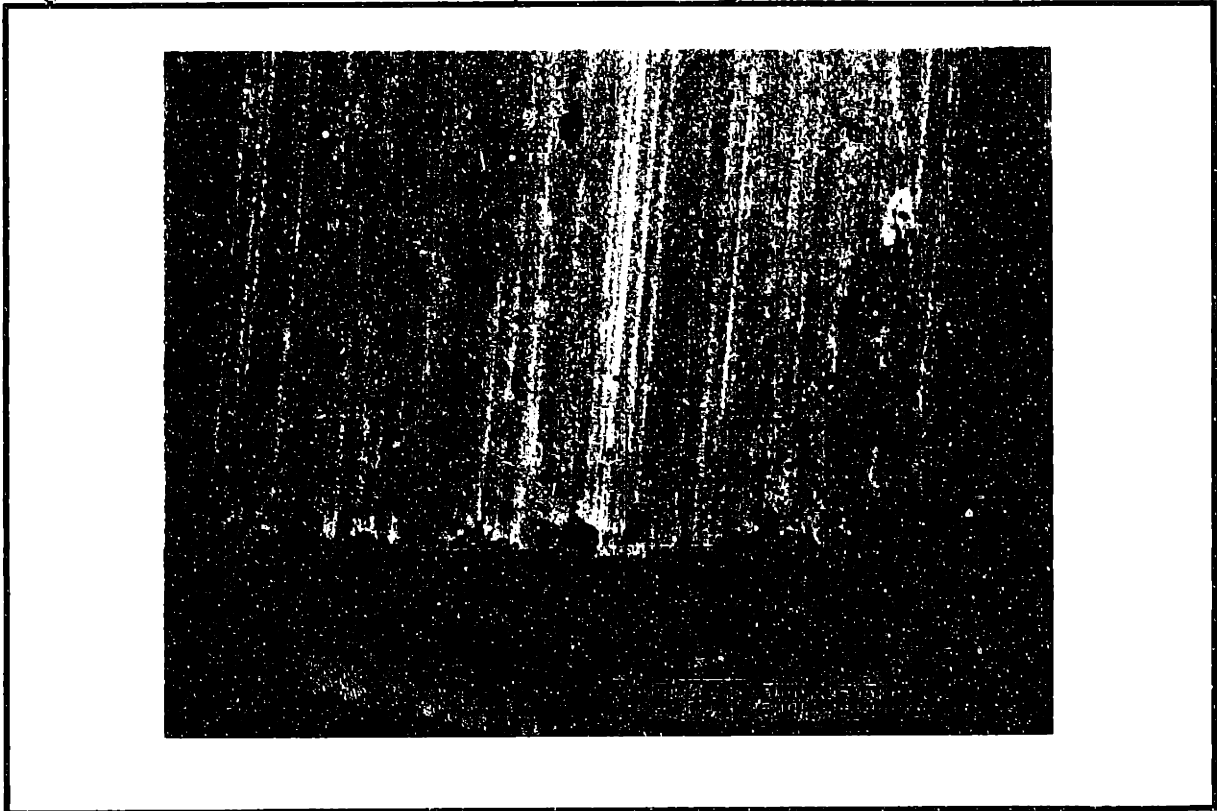


Figure 4.29. The undercut of BLM layer after 86% H_2SO_4 for 3 min.



and lateral direction should theoretically be the same in a linear relationship. However, graphs shown in Figures 4.30 and 4.31 indicate that it is not true for this experiment. First, figure 4.30 shows that the lateral etch rate of the BLM layer is non-linear but seems to have three different stages. For the first two minutes, the etch rate is approximately 2.5 $\mu\text{m}/\text{min}$, showing a very fast etch rate (Figure 4.28). In addition, this rate does not stay the same but gets faster between 2 and 3 minutes, having an etch rate of 8 $\mu\text{m}/\text{min}$. From the graph, the region between 2 and 3 minutes seem to be the most active etch region, resulting in an undercut of 13 μm on both sides of the bump at 3 minutes. Finally, the rate slows down to 1.75 $\mu\text{m}/\text{min}$ between 3 and 5 minutes, having the lowest etch rate. There are several reasons for the nonlinearity of the rate. First, etching is taking place in a few thousand angstrom thick BLM layer

Figure 4.30

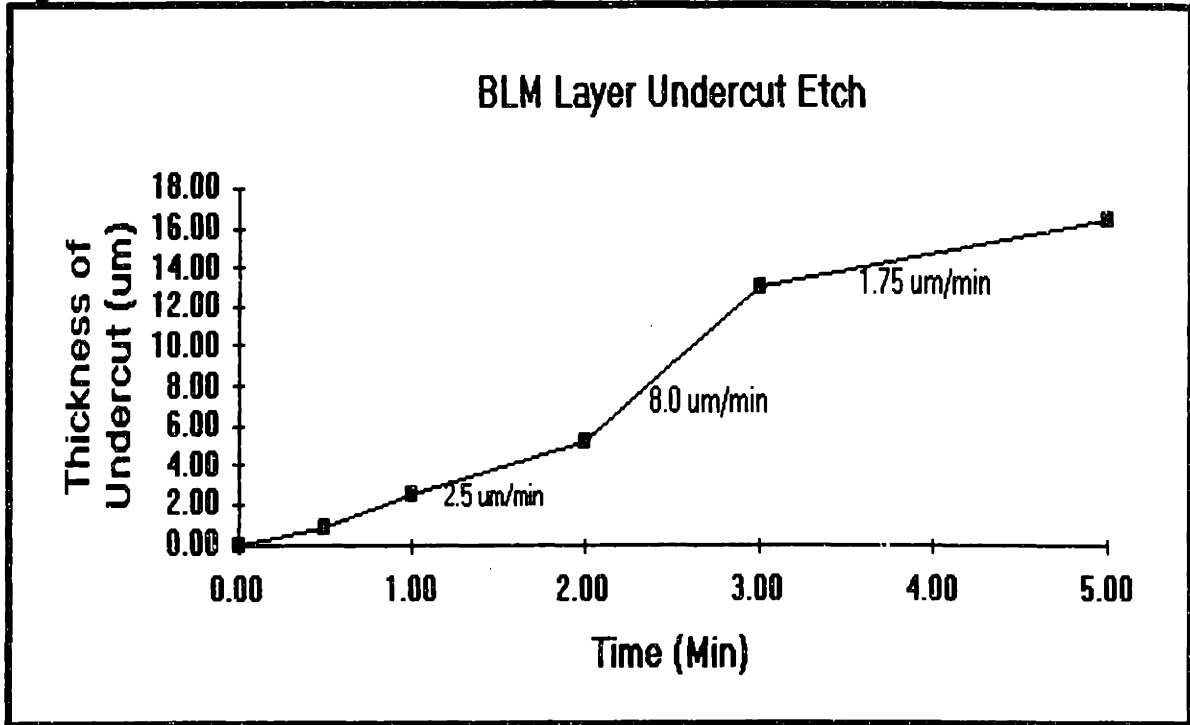
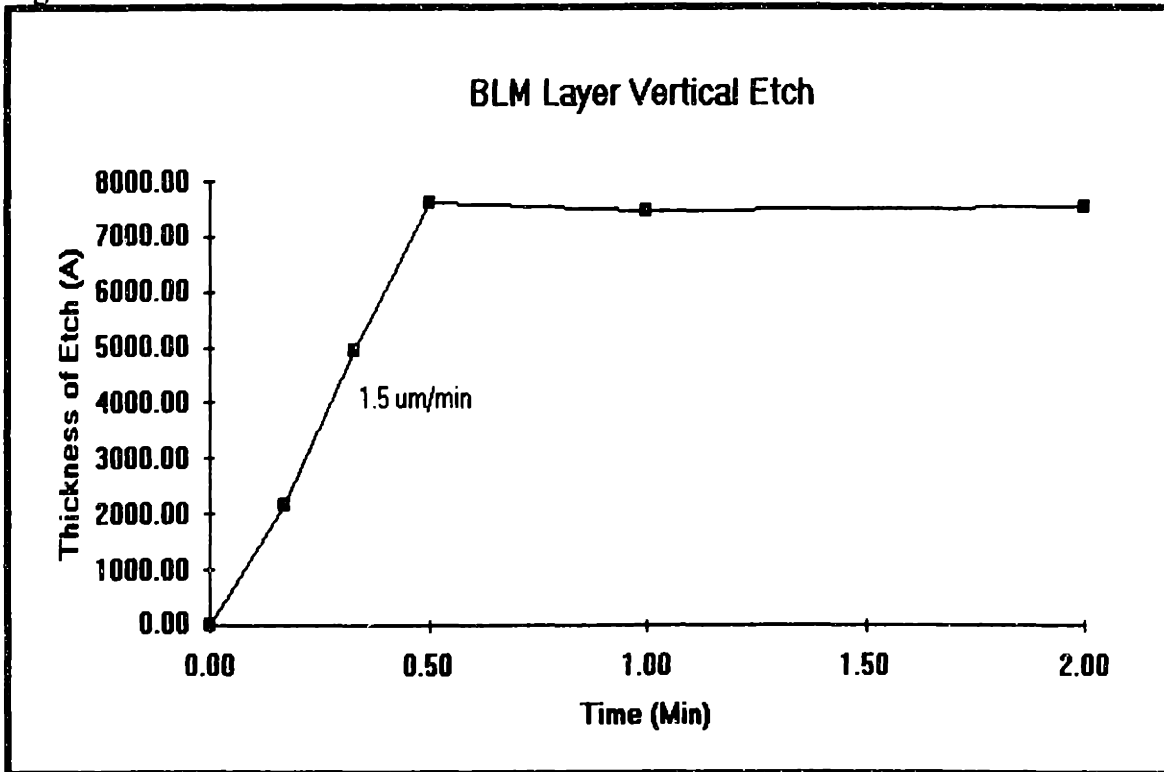


Figure 4.31



space underneath the bump and the liquid flow is constrained by that limited thickness as shown in the SEM picture in figure 4.29. Since the thickness of that layer is so thin, the liquid flow is constrained, reducing the etchant transport therefore, slowing the etch rate. In the second region, the etch rate is the fastest, possibly due to liquid entrapment, that even after rinsing with water, the etching reaction might have continued to occur from the remnants of the etching liquid. Moreover, the third region has the slowest etch rate, possibly due to fluid-flow problems since the deeper the undercut, the more difficult it is for liquid to flow freely through the thin layer. A curve-fitting line over the BLM layer lateral etch rate line showed the etch rate of BLM layer in a lateral direction to be approximately 3 $\mu\text{m}/\text{min}$. Therefore, the overall etch rate in a lateral direction is approximately 3 $\mu\text{m}/\text{min}$. This lateral etch rate has several limitations which allow the etch rate to be inconsistent with theoretical predictions.

Figure 4.31 shows a vertical etch rate of the BLM layer. This etch rate is on a non-bump area as illustrated in figure 4.27. From this graph, it takes about 30 seconds to clear approximately 7700 Å of BLM layer with an etch rate of 1.5 $\mu\text{m}/\text{min}$, half of the etch rate in the lateral direction. After 30 seconds, the etch rate is constant which indicates that there is no BLM layer left to be removed. As shown in the graph, the reaction is linear in relationship since this is a straightforward etch reaction without any constraints. However, the etch rates in vertical and lateral directions are found to be anisotropic. In order for the vertical etch rate to be close to the lateral etch time, the etch time should have been 15 seconds instead of 30 seconds. The delay in the etch time might be due to the experimental error since the wafers were handled manually. Accurate measurement to seconds is difficult when the wafers are handled manually.

These differences between theoretical and experimental results might be due to several reasons, such as fluid flow problems mentioned above, fluid entrapment, the nature of BLM layer materials and the experimental errors due to manual handling of wafers. Moreover, the flow is constrained by a few thousand angstrom thin layer with

Pb/Sn bumps directly over it. This difference between theoretical and experimental results is a significant finding in learning more about etch rates in BLM layer, and further experiments and investigations are required to find out these differences between theoretical and experimental results.

CHAPTER 5. CONCLUSIONS AND RECOMMENDATIONS

5.1. Conclusions

Experiments to identify the effect of various concentrations of BLM etchant solutions on Pb/Sn solder bumps were performed. A thin surface layer was observed to be formed during the etching operation. This thin layer prevented the melting and the reflow of the bumps during subsequent thermal treatment operation. The reaction kinetics, composition and morphology of this layer were studied using various techniques. Based on these results, an etch chemistry was determined to remove this surface layer.

Morphology and composition of the surface layer on Pb/Sn solder bumps:

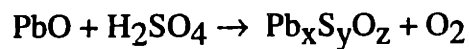
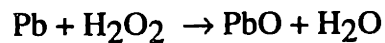
The impact of BLM etchant on the morphology of surface layer was studied. It was found that the morphology was critically dependent on the etchant concentration, especially H_2SO_4 . In H_2SO_4 -rich solutions, the layer on the Pb/Sn solder bumps was very thin and dense as shown in Figures 4.1 and 4.2. However, as the concentration of H_2O_2 relative to H_2SO_4 increased, the layer appeared to be more loosely (Figure 4.3-4.4). However, the morphology of the surface layer was independent of the etch time although the thickness increased with time. Also, the layer on the surface appeared to be composed of multiple thin layers.

Several methods were attempted to identify the compound on the surface of solder bumps; XPS, AES, RBS, EDX, XRF and AFM. Only AES and XPS were found to give meaningful data in the current study. However, it must be noted that AES does not provide information about bonding state and XPS peak shifts due to charging. Pb, S, O and Sn were identified as the primary components of the surface layer. AES indicated a 10% increase in S in layers produced with sulfuric rich etchant compared to those produced in peroxide-rich solution. XPS data interpretation was difficult because of the overlapping binding energy peaks between Pb^{2+} and Pb^{4+} . So a clear determination of

the exact nature of the surface layer could not be made. Gravimetric testing was used to identify the primary composition of the surface layer. The Pourbaix diagram from the literature was used to explain a different regime of stability for PbO, PbO₂ and Pb₃O₄. PbO, PbO₂ and Pb₃O₄ were dissolved in the acid under various conditions. Based on all of these tests, Sn, S containing PbO, was found to be the compound on the surface after 86% H₂SO₄ BLM etch bath. The final pH of the solution with the acid, that was used to clean the bumps for reflow, was found to be about 6.03. The initial pH of the diluted 10% acid was -0.53. This result matches closely with the Pourbaix diagram which determines a pH and electrode potential of the solution at the stability of different Pb compounds in the solution. The maximum solubility found in the diluted 10% acid was approximately 1.82M. Using 50% concentrated acid with an initial pH of -1.02, the whole solution becomes a block of dense, white crystals, showing the highest solubility of 747.5 g/l. PbO consumed all the acid solution, with a final concentration of approximately 3M. The solubility tends to increase as the final pH decreases from the pH level of 6.03 and the solubility tends to decrease as the final pH increases (Table 4.5).

Reaction mechanism of Pb/Sn solder bumps in high and low sulfuric concentration: The impact of the BLM etch bath on Pb/Sn solder bumps were investigated. As seen from Figure 4.25, the surface layer thickness was found to be proportional to the etch time in the H₂O₂-rich solution. This layer growth would be a reaction rate limited with a growth rate of 1.1 um/min in the H₂O₂-rich solution. However, in the H₂SO₄-rich solution, the thickness of the surface layer is proportional to the square root of the time as seen in Figure 4.26. This suggests a diffusion rate limited growth. This agrees with the thickness morphology studies that S is the primary reason for the differences in morphology. More studies were done by varying the concentration of H₂O₂ and H₂SO₄ (Figure 4.13 & 4.14). From these studies, it was determined that the H₂O₂-rich region has reaction 2nd order when the H₂SO₄-rich region is a zero order of reaction. Also, neither H₂O₂ nor H₂SO₄ alone can etch the BLM layer. A

combination of these two solutions is needed to create a thin layer on the surface of solder bumps and to etch the BLM layer at the same time. The H_2O_2 tends to produce a faster, thicker surface layer of formation than that of H_2SO_4 where a dense and thin surface layer is formed. The region between 35% and 85% H_2SO_4 seems to be the most favorable area where the surface layer thickness is less than 5 μm after 4 minutes and the BLM layer gets etched as well. The optimum etch bath was found to be a 86% H_2SO_4 solution where the resulting thickness of the surface layer was about 1 μm with a noticeable undercut in the BLM layer after 4 minutes of etch. In this solution, the diffusion rate is the controlling step in the slow formation of the surface layer. Based on these results, we propose the following reaction:



BLM Layer Etch rate studies: After discovering the optimal concentration for the BLM etch bath, the etch rate of BLM layer was investigated (Figures 4.30 & 4.31). In contrast to the theoretical predictions, where the etch rate in the vertical and the lateral directions is an isotropic reaction and should be the same, the two etch rates were found to be anisotropic. The etch rate in a lateral direction was not only non-linear but seemed to show three different etch rates between 0 and 5 minutes. The overall etch rate was determined to be approximately 3 $\mu\text{m}/\text{min}$. These etch rate differences might be due to fluid flow problems, liquid entrapment and the metallurgical properties of the BLM layer. Also, the etch rate in a vertical direction was determined to be 1.5 $\mu\text{m}/\text{min}$, where the overall etch rate was half of that in the lateral direction. Fluid flow related issues and liquid entrapment could be the primary reasons why the overall etch rate is slower in a vertical direction than in a lateral direction. Also, experimental error caused by the manual handling of the wafers might be a contributor to the differences between the

lateral and the vertical etch rate. Thus, the experimental etch rate was found to be anisotropic.

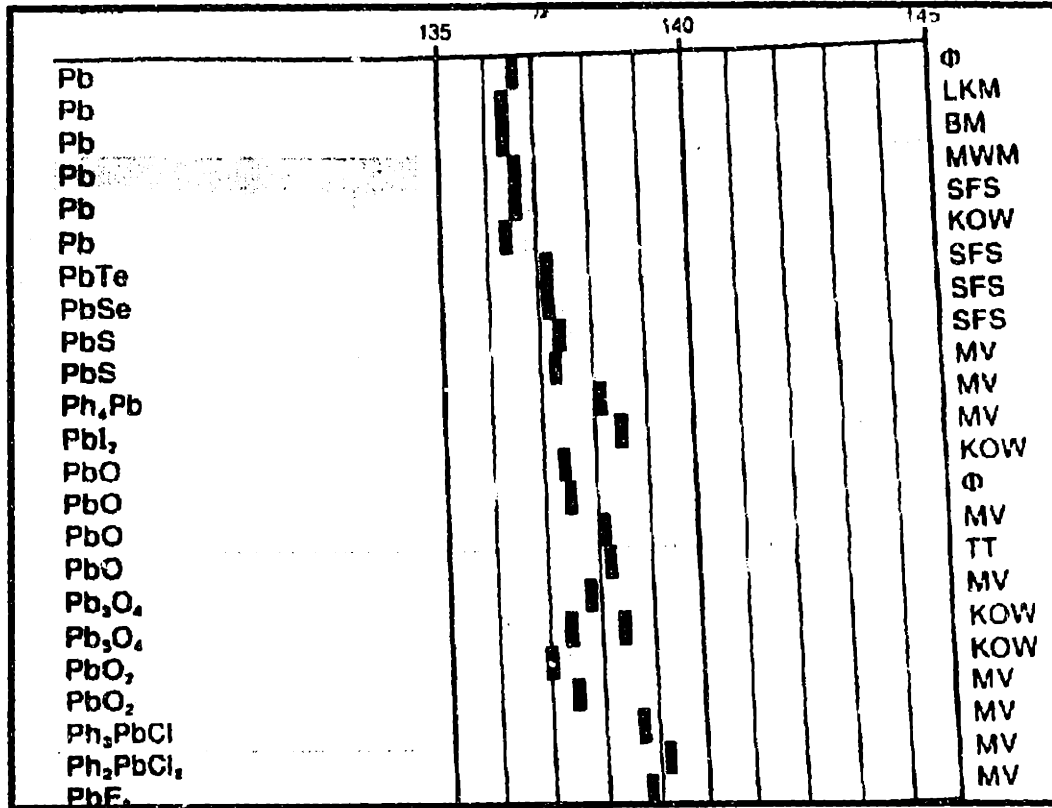
Overall, several findings were concluded. First, BLM layers were selectively etched after oxidizing the Pb/Sn bumps using H_2SO_4 and H_2O_2 . Second, to identify the composition of the oxides on the Pb/Sn bumps, several spectroscopic techniques were used but some limitations, such as overlap between Pb and S peak, and very close binding energy of Pb^{2+} and Pb^{4+} , narrowed down to XPS and AES only. Third, the Pourbaix diagram using gravimetric test was used to overcome the limitations of spectroscopic techniques. This diagram for Pb was able to show which Pb compound the bulk material of the surface layer was composed of. Finally, the etch rate of BLM layer in a vertical and lateral directions were studied using SEM and Omnimap, and the experimental etch rate was found to be anisotropic.

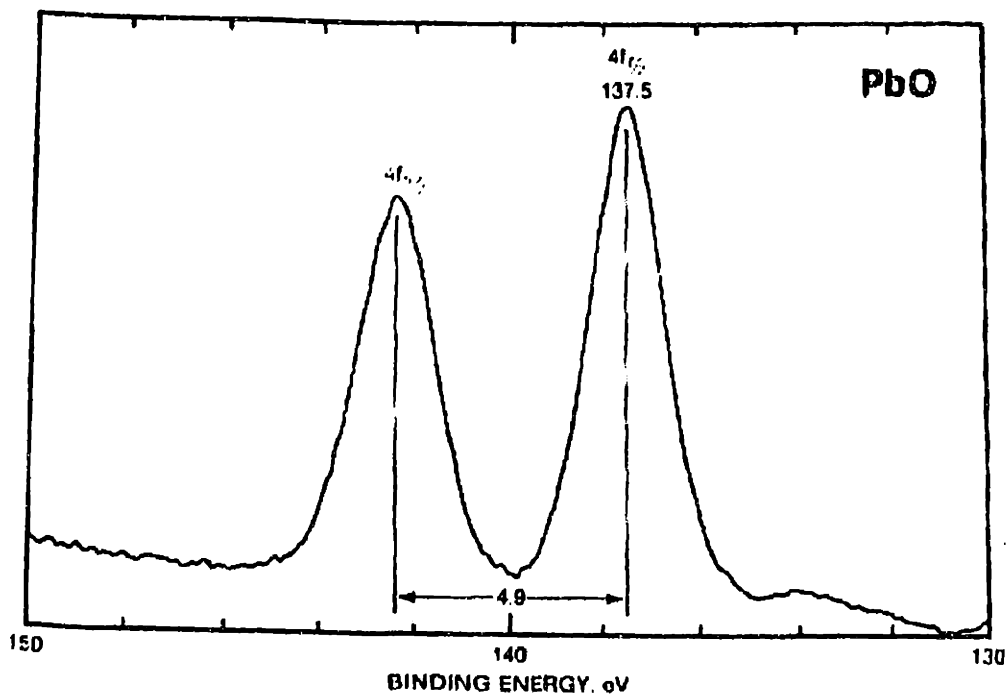
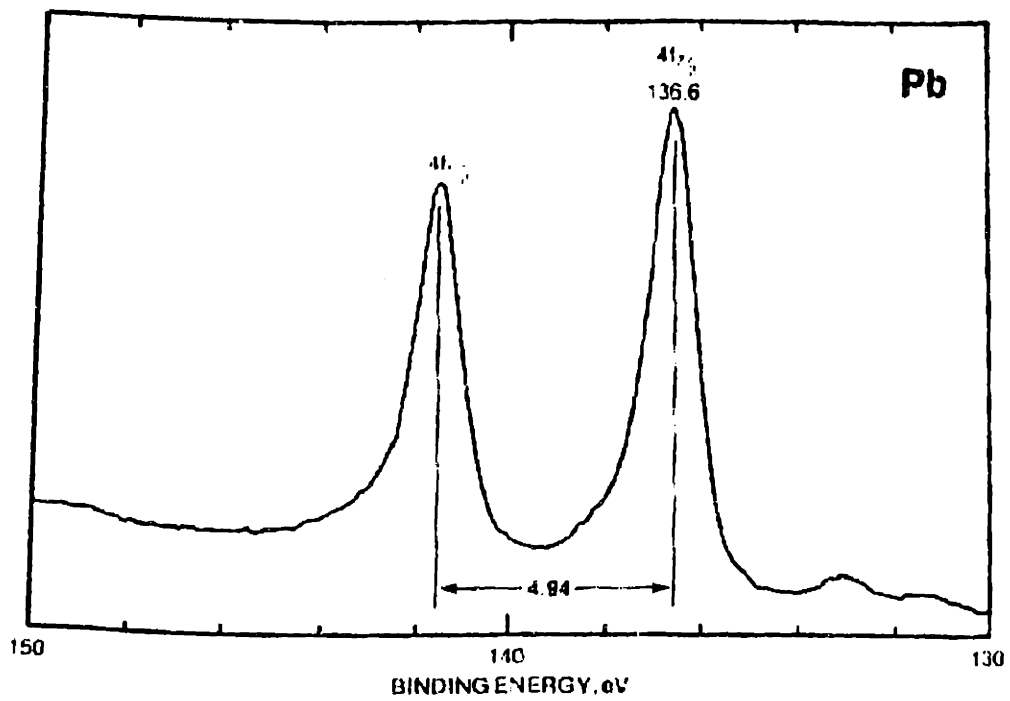
5.2. Recommendations

There are several areas for future work that could be pursued. The precision cross-section and gravimetric tests need to be further refined to make them more sensitive. Also, more studies need to be done on the BLM layer etch rate studies. The experiment needs to be more controlled than the present method used in order to understand the root cause of the etch rate differences.

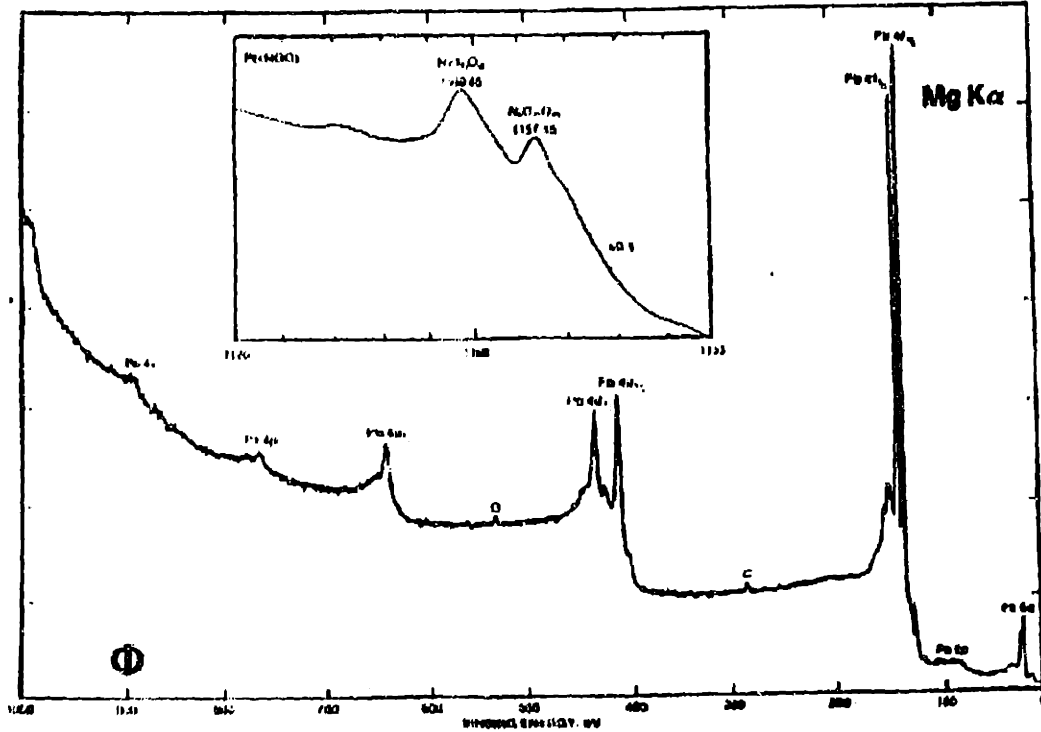
APPENDIX I

Binding Energy (eV) of Pb compounds





Lead, Pb $Z=82$

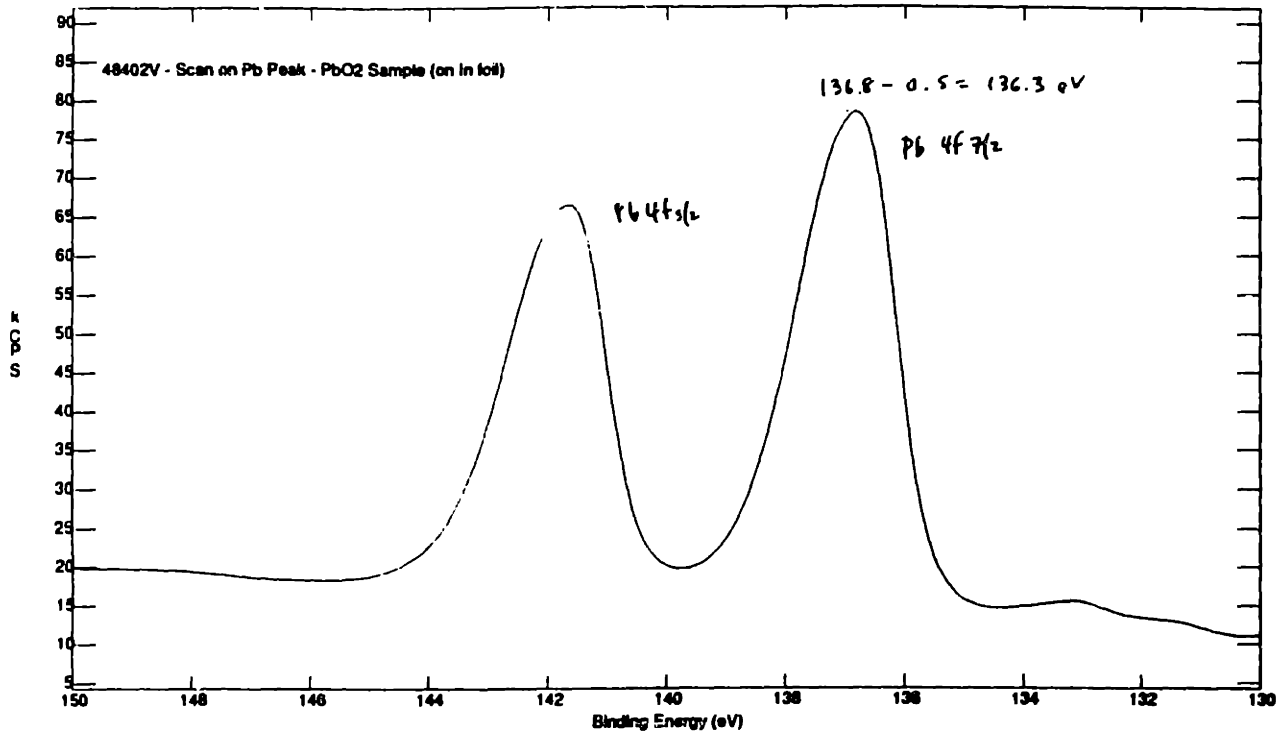


[Source: Handbook of X-ray Photoelectron Spectroscopy, pp. 160]

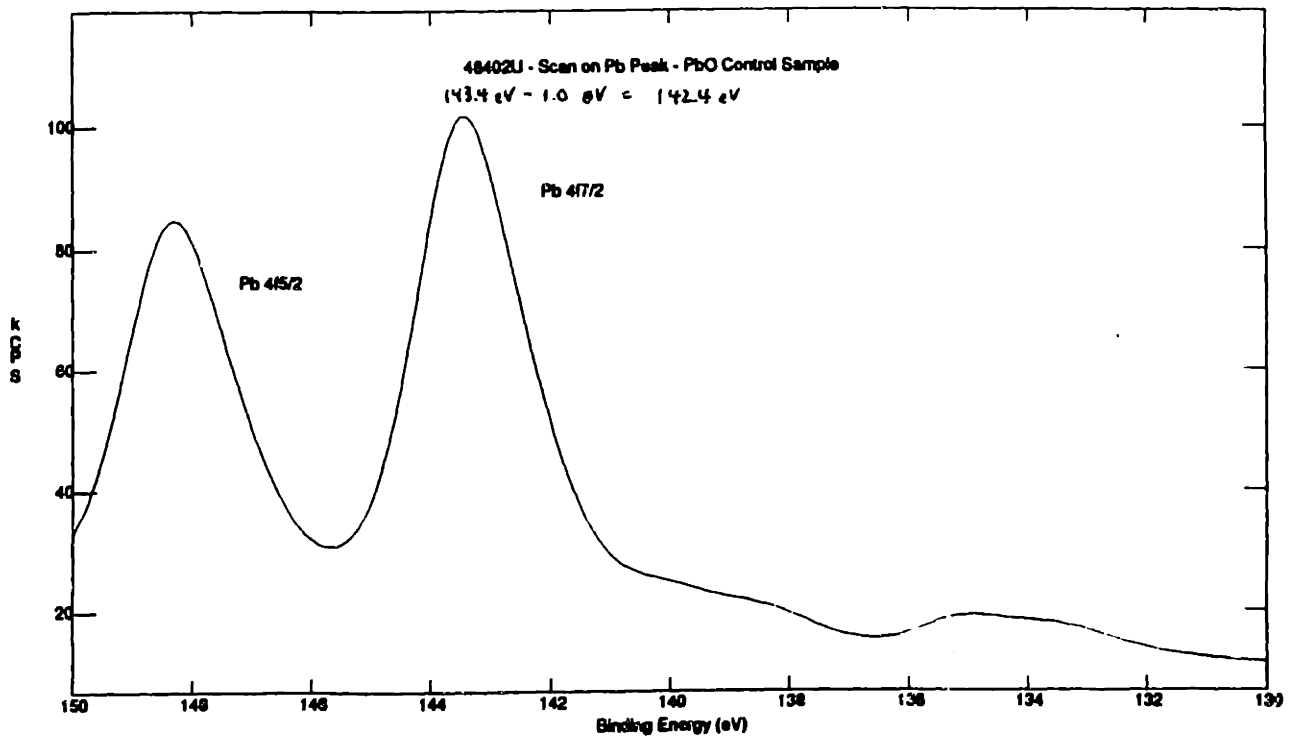
APPENDIX II

XPS Results of Pb compounds

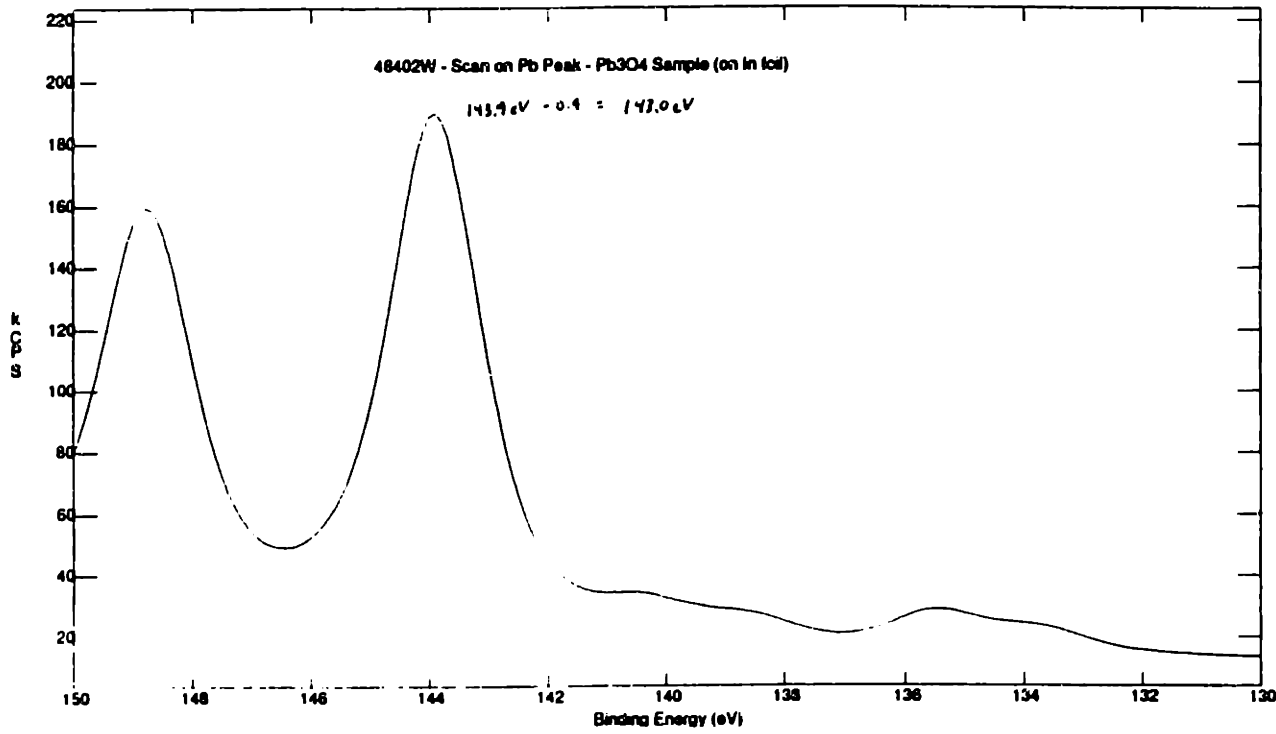
XPS ANALYSER	R00002 C:148402VLR00002	08-12-1993
SOURCE	CAE = 20eV STEP = 100 meV SCANS = 200 TIME = 1h 7m 0.00s	
LABEL	Mg K-alpha	
	48402 - Survey, high res scans on PbO2 sample (on In Foil)	FISONS



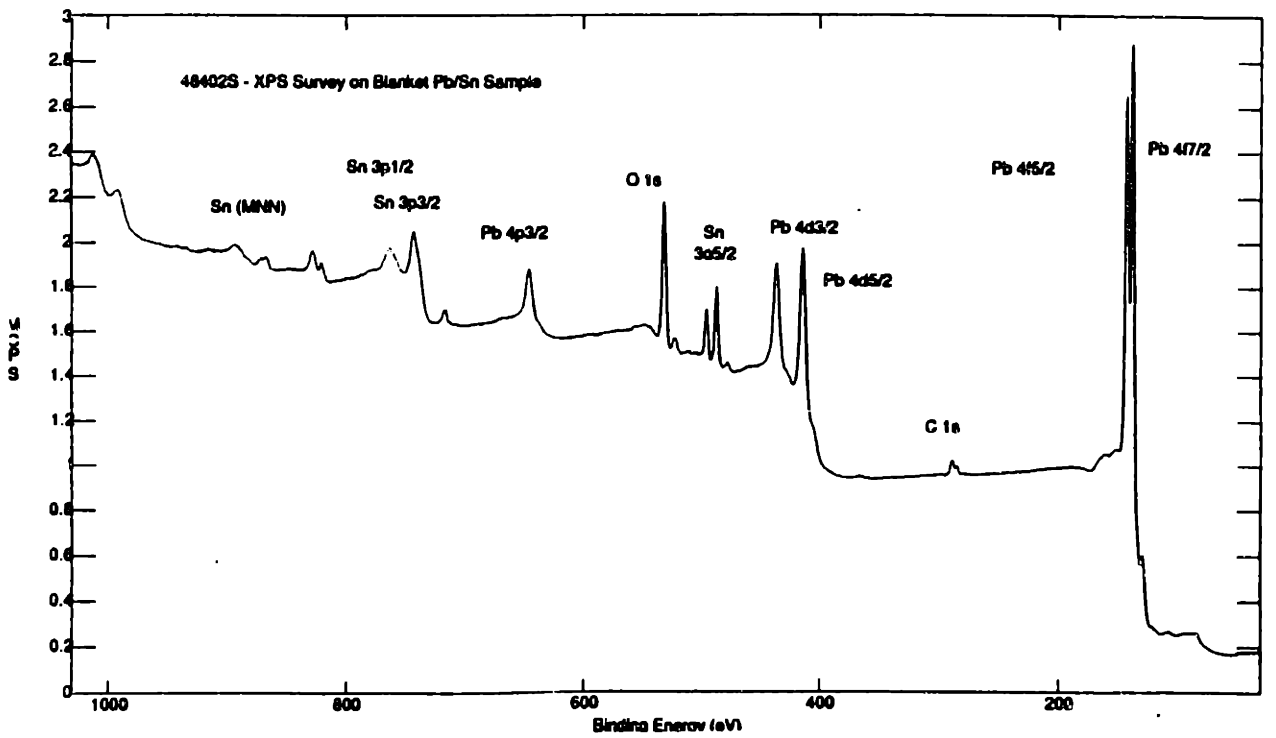
XPS ANALYSER	R00002 C:148402LNR00002	07-12-1993
SOURCE	CAE = 20eV STEP = 100 meV SCANS = 200 TIME = 1h 7m 0.00s	
LABEL	Mg K-alpha	
	48402 - Survey on PbO Sample	FISONS



XPS ANALYSER R00002 C:\48402W\R00002 13-12-1993
 SOURCE CAE = 20eV STEP = 100 meV SCANS = 200 TIME = 1h 7m 0.00s
 LABEL Mg K-alpha 48402 - XPS Survey and high res scan on Pb3O4 Sample

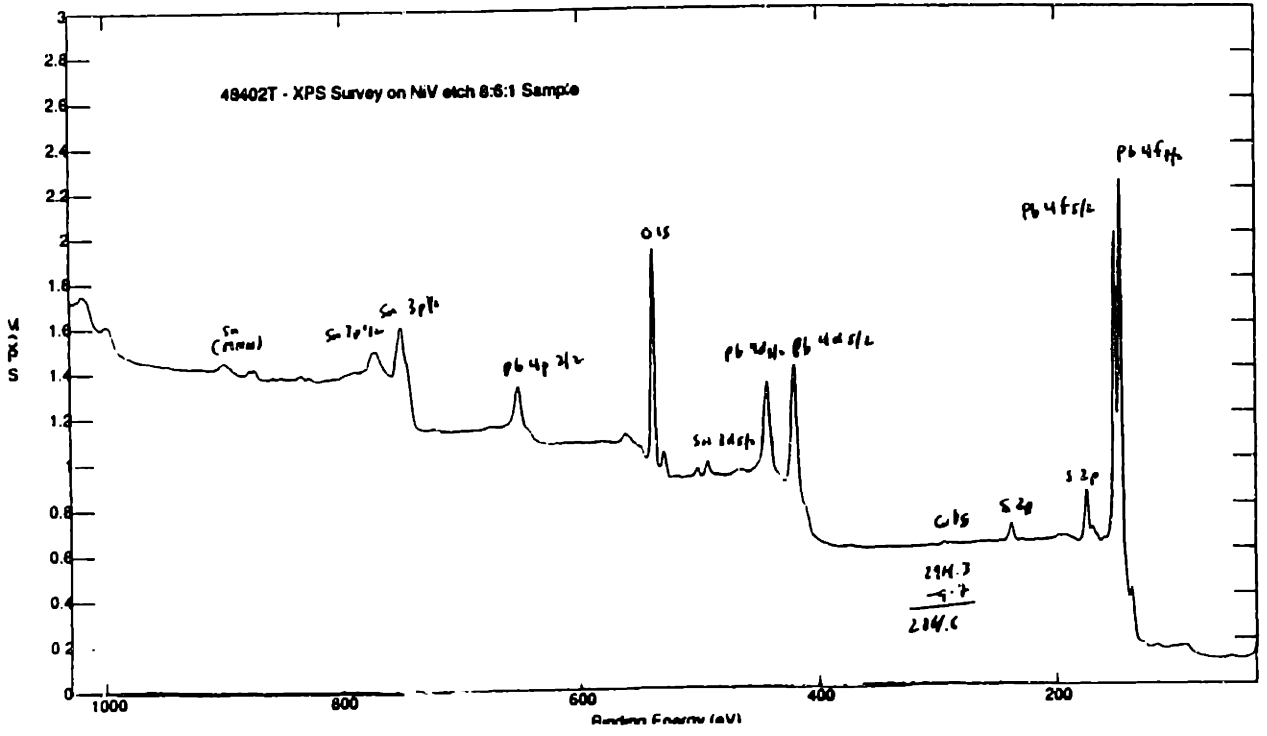


XPS ANALYSER R00001 C:\48402S\R00001 02-12-1993
 SOURCE CAE = 100eV STEP = 489.005 meV SCANS = 10 TIME = 8m 1.40s
 LABEL Mg K-alpha 48402 - XPS Survey and High resolution scan on Pb/Sn Blanket Water



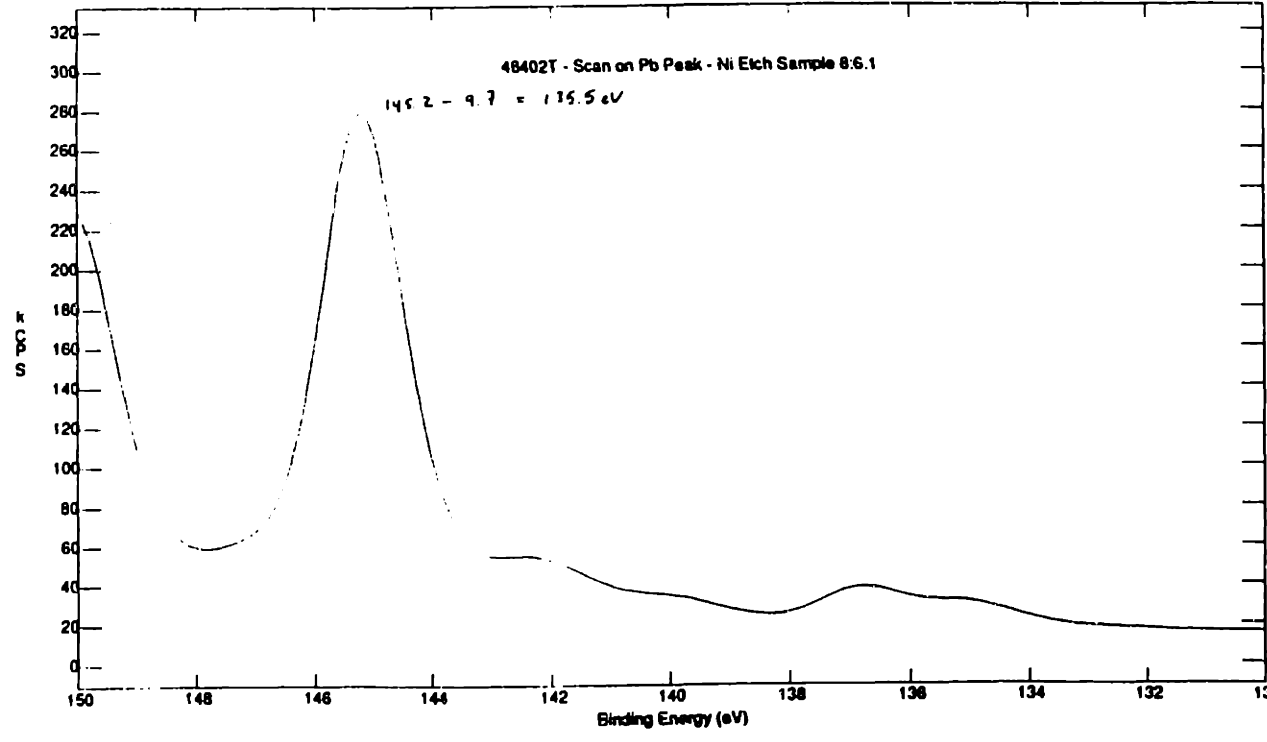
XPS ANALYSER SOURCE LABEL
 R00001 C:48402TR00001
 CAE = 100eV STEP = 500.083 meV SCANS = 10 TIME = 8m 0.20s
 Mg K-alpha
 48402 - C. Lee - Ni/Ti Etch 8:8:1 XPS Survey, high res scan

03-12-1993
FISONS



XPS ANALYSER SOURCE LABEL
 R00002 C:48402TR00002
 CAE = 20eV STEP = 100 meV SCANS = 200 TIME = 1h 7m 0.00s
 Mg K-alpha
 48402 - C. Lee - Ni/Ti Etch 8:8:1 XPS Survey, high res scan

03-12-1993
FISONS



APPENDIX III

Thermodynamic Properties of Pb compounds

Formula and Description	ΔH_f	ΔG_f	S	C_D
PbO (red)	-52.34	-45.23	15.9	10.94
PbO (yellow)	-52.12	-45.09	16.42	10.94
PbO ₂	-65.6	-51.5	17.16	14.62
Pb ₂ O ₃			36.3	25.74
Pb ₃ O ₄	-171.8	-143.8	50.7	37.03
PbS	-23.50	-23.12	21.83	11.82
PbSO ₄	-219.87	-194.36	35.51	24.67

[source: Lange's Handbook of Chemistry, 1956, pp. 9-31 - 9-32]

REFERENCES

- Bendz, D.J., Gedney, R.W. and Rasile, J. , "Cost/Performance Single-Chip Module", *IBM J. Res. Develop.*, 24(3): pp. 278-285, May 1982.
- Bowlby, R., "Finish First", *SMT soldering*, Nov. 1987.
- Cavanaugh, D.M., "Thermal comparison of Flip-chip relative to Chip-and-wire semiconductor attachment in hybrid circuits: An experimental approach", *ISHM Proc.* pp. 214 - 219, Sept. 1975.
- Charles, H.K., Jr. "Electrical Interconnection", *Electronic Materials Handbook, Vol.1: Packaging*. Materials park, OH: ASM International, 1989.
- Clatterbaugh, G.V. and Charles, Jr., H.K., "Design Optimization and Reliability Testing of Surface Mounted Solder Joints", *Proceedings of the 1985 International Symposium on Microelectronics*, pp. 31-42, Nov. 1985.
- Chu, R.C., Hwang, U.P. and Simons, R.E., "Conduction Cooling for an LSI Package: A one-dimensional Approach", *IBM J. Res. Develop.*, 26 (1) pp. 45-54, Jan. 1982.
- Goldmann, L.S., "Geometric Optimization of Controlled Collapse Interconnections", *IBM J. Res. Develop.*, pp. 251-265, May 1969.
- Goldmann, L.S., "Self-alignment Capability of Controlled-Collapse Chip joining", *Proceedings 22nd Electronic Comp. conf.*, pp. 332-339, May 1972.
- Goldmann, L.S., Herdzyk, R.D., Koopman, N.G. and Marcotte, V.C., "Lead-Indium for Controlled-Collapse Chip Joining", *IEEE Transactions on Parts, Hybrids, and Packaging*, Vol. PHP-13(3), pp. 194-198, Sept. 1977.
- Goldmann, L.S. and Totta, P.A., "Area Array Solder Interconnections for VLSI", *Solid State Technology*, pp.91-97, June 1983.
- Howard, R.T., "Optimization of Indium-Lead Alloys for Controlled Collapse Chip Connection Application", *IBM J. Res. Develop.*, 26 (3): pp. 372-378, May 1982.
- Jackson, R.L., Carnevali, P. and Frazier, J.D., "Finite-Element Modeling of Encapsulated Flip-Chip Packaging Assemblies", *ISHM '91 Proceedings*, pp.82-85, 1991.
- Kamei, T., Nakamura, M., Ariyoshi, H. and Doken, M., "Hybrid IC Structures using Solder Reflow Technology", *'78 Proceedings, 28th ECC*, pp. 172-182, 1978.

- Kawanobe, T., Miyamoto, K., Inaba, Y. "Solder bump Fabrication by electrochemical Method for Flip Chip interconnection", *IEEE*, pp. 149-155, 1981.
- Lange, N.A., "Lange's Handbook of Chemistry", McGraw-Hill Book Company, New York, 1956.
- Lowenheim, F.A., "Electroplating: Fundamentals of Surface Finishing", McGraw-Hill Book Company, New York, 1978.
- Miller, L.F., "Joining Semiconductor Devices with Ductile Pads", *1968 Hybrid Microelectronics Symposium*, Chicago, pp.333-342, Oct. 29, 1968.
- Miller, L.F. "Controlled Collapse Reflow Chip Joining", *IBM J. Res. Develop.*, pp. 239-250, May 1969.
- Myers, T.R., "Flip-Chip Microcircuit Bonding Systems", *Proceedings.1969 ECC*, pp.131-144, 1969.
- Nagesh, V.K., "Reliability of Flip Chip Solder Bump Joints", *Reliability Physics Symposium*, pp. 6-15, 1982.
- Norris, K.C. and Landzberg, A.H., "Reliability of Controlled Collapse Interconnections", *IBM J. Res. Develop.*, 13 (3): pp.266-271, May 1969.
- Ohshima, M., Kenmotsu, A. and Ishi, Ichiro, "Optimization of Micro solder Reflow Bonding for the LSI flip chip", *The second International Electronics packaging Conferences*, pp.481-488, Nov.1982.
- Oktay, S., "Parametric Study of Temperature Profiles in chips joined by controlled collapse techniques", *IBM J. Res. Develop.*, pp. 272-285, May 1969.
- Oktay, S. and Kammerer, H.C., "A conduction-Cooled Module for High-Performance LSI Devices", *IBM J. Res. Develop.*, 26(1) pp. 55-66, Jan. 1982.
- Pourbaix, Marcel, "Atlas of Electrochemical Equilibria In Aqueous Solutions", National Association of Corrosion Engineers, Houston, 1974.
- Puttlitz, K.J. "Preparation, Structure, and Fracture Modes of Pb-Sn and Pb-In Terminated Flip Chips Attached to Gold-Capped Microsockets", *40th Electronic Components & Technology Conference*, pp. 360-367, May 1990.
- Reed-Hill, Robert E. and Abbaschian, R., "Physical Metallurgy Principles" PWS-KENT publishing company, Boston, 1973.

Sun, S.P., Wu, F. "The progress of Flip Chip Technology", Microrobotics systems, Inc. MA., pp. 1-8

Takenaka, T., Kobayashi, F. and Netsu, T., "Reliability of Flip-chip interconnections", *1984 ISHM Conf. Proc.*, pp.419-423, Sept. 1984.

Thibeau, R.J. and Brown, C.W., "Corrosion Films on Lead in 0.1 M Sulfate Solutions", *Journal of electrochemical society*, 27(9): pp. 1913-1918, Sept. 1980.

Totta, P.A., "Flip Chip Solder Terminals", *21st Electronics Components Conf.*, pp. 275-284, May 1971.

Tuck, John. "In Search of Flip Chip", *Circuits Assembly*, pp 22-24, April 1992.

Tumala, R., Rymaszewski, E.R. *Microelectronics Packaging Handbook*, Van Nostrand Reinhold, New York, ch. 6, pp.361-391, 1989.

Wolf, J., Chmiel, G. and Reichl, H., "Lead/Tin (95/5 wt%)-solder bumps with Ti:W/Au/Cu Under Bump Metallization", *ITAP '93 Proceedings*, pp.141-152, 1993.

Wolf, S. and Tauber, R.N. "Silicon Processing for the VLSI Era, Volume 1", Lattice Press, California, 1986.

Yung, E.K., Turlik, I. "Electroplated Solder Joints for Flip Chip Applications", *IEEE Transactions on components, hybrids, and manufacturing technology*, 14(3): pp.549-559, Sep.1991.